XAPT and XLPT enzymes modify the glucuronic acid side chains of tissue-specific xylans in Arabidopsis and Eucalyptus

Li Yu[1#], Louis F.L. Wilson[1#], Oliver M. Terrett[1#], Joel Wurman-Rodrich[1], Jan J. Lyczakowski[1], Xiaolan Yu[1], Kristian B.R.M. Krogh[2], Paul Dupree[1*]

[1] Department of Biochemistry, University of Cambridge, Hopkins Building, The Downing Site, Tennis Court Road, Cambridge CB2 1QW, UK

[2] Novozymes A/S, Krogshøjvej 36, 2880 Bagsværd, Denmark

[#] These authors contributed equally to this paper.

[*]Corresponding author: Paul Dupree Phone number: (44)1223 333340

Email: pd101@cam.ac.uk

This manuscript includes: 6495 words; 8 Coloured Figures, 12 Supplemental Figures and 1 Supplemental Table.

Summary

- Plant cell wall polysaccharides such as xylan not only contribute to cell shape, but also hinder pathogenic and biotechnological attempts to saccharify the wall. This recalcitrance derives substantially from polysaccharide structural complexity, driven by biosynthetic glycosyltransferases. Glucuronic acid sidechains along the xylan backbone can be further decorated with arabinopyranose or galactose in certain tissues and species. We sought to identify the responsible glycosyltransferases.
- We identified the relevant locus from candidate Arabidopsis mutants by polysaccharide profiling and reverse genetics. We demonstrated different activities of two paralogues in eucalyptus by heterologous expression and investigated this neofunctionalisation by molecular phylogeny. Finally, we measured the activities of various GH30-family *endo*-glucuronoxylanases on modified xylans *in vitro*.
- *At*XAPT1 (AT1G68470) and *Eg*XAPT (Eucgr.D00738) encode Xylan ArabinoPyranosylTransferases, whereas *Eg*XLPT (Eucgr.H00343) encodes a Xylan GalactoPyranosylTransferase. While arabinopyranosyl decorations in native eucalyptus appear to be enriched in primary walls, overexpression of the eucalyptus enzymes in Arabidopsis can accomplish substantial changes in secondary wall xylan structure. Only some GH30 glucuronoxylanases have evolved to accommodate substituted glucuronic acid, perhaps through a single active site substitution.
- Our results demonstrate the adaptability of biosynthetic and degradative carbohydrate-active enzyme activities, providing insight into a plant-pathogen arms race and facilitating wall biotechnological utilisation.

Key words: biosynthesis, cell wall, glycosyltransferase, neofunctionalisation, XAPT, xylan, xylanase

Introduction

The plant cell wall is an extracellular matrix that surrounds every plant cell (Burton *et al.*, 2010). Depending on the cell type, the cell wall supports the upright growth of the plant and acts as a complex physical barrier that protects the cell from abiotic and biotic stress. Cell walls are composed of a mixture of polysaccharides, phenolic polymers, and proteins whose composition varies considerably between different plants (Burton *et al.*, 2010). The structural complexity of cell walls is thought to contribute to cell wall properties, including their resistance to degradation by pathogens, and the different structures of polysaccharides may shape the properties of different cell types and tissues.

Forming a common hemicellulosic component of plant cell walls, xylan polysaccharides are thought to bind to and thus chaperone cellulose microfibrils (Busse-Wicher *et al.*, 2014; Simmons *et al.*, 2016) and mediate cross-links to other cell wall components (Terrett & Dupree, 2019; Tryfona *et al.*, 2023). Xylans vary in structure between different species and tissues, but invariably they possess a backbone of β1,4-linked xylosyl residues (Scheller & Ulvskov, 2010). In Arabidopsis and other eudicots, the xylan backbone is typically decorated with side groups of 2/3-linked acetate and α1,2-linked glucuronic acid (GlcA), which is often 4-*O*-methylated. The spacing of these decorations along the xylan backbone is critical for regulating its interaction with cellulose microfibrils (Simmons *et al.*, 2016; Grantham *et al.*, 2017; Tryfona *et al.*, 2023). While most xylan in Arabidopsis is present in the secondary cell wall (SCW), it also makes up part of the primary cell wall (PCW) (Mortimer *et al.*, 2015). Although the function of PCW xylan has not been determined, plants appear to allocate dedicated machinery to synthesise it: whereas the SCW xylan backbone is synthesised by IRX9, IRX10, and IRX14/14L, PCW xylan is synthesised specifically by IRX9L, IRX10L, and IRX14 (Mortimer *et al.*, 2015; Anders *et al.*, 2022). Furthermore, the pattern of GlcA decoration differs substantially between PCW and SCW xylan. SCW xylan glucuronidation is achieved by two enzymes: GUX1, which produces an even-spaced pattern, and GUX2, which produces a more random pattern of GlcA side chains (Bromley *et al.*, 2013). In contrast, PCW xylan is glucuronidated consistently at every sixth backbone xylosyl residue by GUX3 (Mortimer *et al.*, 2015). Notably, in at least some PCW-rich Arabidopsis tissues, the GlcA moieties of PCW xylan can be further decorated with a pentose that has been assigned as a putative α1,2-linked L-arabinopyranose (Ara*p*) (Chong *et al.*, 2015; Mortimer *et al.*, 2015). The glycosyltransferase responsible for this decoration has not yet been identified, hindering

investigations into the functions of these Ara*p*-α1,2-GlcA-α1,2- ($U^{Ara\,p}$) disaccharide sidechains.

Prior to its discovery in Arabidopsis, decoration of xylan GlcA residues with additional sugars was previously observed for several species in the *Eucalyptus* genus of the Myrtaceae family (Shatalov *et al.*, 1999; Evtuguin *et al.*, 2003; Pinto *et al.*, 2005). Interestingly, further experiments showed unequivocally that the GlcA residues in Eucalyptus xylan can not only be substituted with α1,2-linked L-Ara*p* (as thought to be the case in Arabidopsis) but also with a sterically similar moiety, β1,2-linked D-galactose (Gal) (Togashi *et al.*, 2009; Pena *et al.*, 2016). Furthermore, the $U^{Ara\,p}$ sidechain has also been shown to be widely present in xylans from non-commelinid monocots (Pena *et al.*, 2016). However, whether the Gal-β1,2-GlcA-α1,2- (U^{Gal}) sidechain is present in plants outside the *Eucalyptus* genus is unknown.

Similar disaccharide side chains with terminal β1,2-linked galactose can be found in several other widespread PCW hemicelluloses. For example, the glucan backbone of xyloglucan—the most abundant hemicellulose in eudicot PCWs—is frequently substituted with a Gal-β1,2-Xyl-α1,6- disaccharide (Scheller & Ulvskov, 2010). Similarly, the backbone mannosyl residues of β-galactoglucomannan (β-GGM) can be substituted with a Gal-β1,2-Gal-α1,6-disaccharide (Yu *et al.*, 2022). The galactosyl residue on xyloglucan side chains is essential for normal morphology, and mutant plants lacking these residues exhibit severely stunted growth (Tamura *et al.*, 2005); furthermore, this phenotype can be exacerbated by removing the analogous galactosyl residues from β-GGM (Yu *et al.*, 2022). Although the mechanism for this phenotype has not been completely clarified, these phenotypes may result from self-aggregation of xyloglucan in the absence of the galactosyl side chains (Kong *et al.*, 2015; Han *et al.*, 2020). However, galactose itself is not specifically required for xyloglucan function, as normal growth of these galactosylation mutants can be restored by replacing the missing galactosyl residues with α-L-arabinofuranosyl, α-L-arabinopyranosyl, or β-xylopyranosyl moieties (Schultink *et al.*, 2013; Zhu *et al.*, 2018; Immelmann *et al.*, 2023; Wilson *et al.*, 2023).

As well as contributing to the material properties of the cell wall, PCW hemicelluloses pose an obstacle to invading pathogens. Pathogens—as well as saprophytes and xylan-degrading gut micro-organisms—must therefore secrete cell wall-degrading glycosyl hydrolases (GHs) in order to gain access to the cell. To overcome the barrier posed by xylan, fungal and bacterial pathogens typically secrete *endo*-xylanases—the best studied being from CAZy

families GH5, 8, 10, 11, and 30 (Paes *et al.*, 2012). Different families differ in their substrate specificities: whereas GH8, 10, and 11 tend to cut preferentially at unsubstituted regions of the xylan backbone, GH5 xylanases are typically arabinoxylan-specific, and most characterised GH30 xylanases require a GlcA-substituted xylosyl residue at the −2 subsite. Efficient xylan digestion is dependent on additional glycosidases that remove obstructive backbone decorations and/or help to break down the resultant oligosaccharides (α-glucuronidases from family GH115, for instance); therefore, a pathogen's ability to digest xylan is limited by the GH activities it can produce. For these reasons, the additional structural complexity provided by side chains in xylan and other PCW hemicelluloses may limit degradation. Indeed, xylanases active on simpler birch wood xylans have been shown to be less effective at hydrolysing complex corn xylan (Rogowski *et al.*, 2015). Xylanase activity is thought to be an important part of infection by disease-causing microbes (Bellincampi *et al.*, 2014). Supporting this, cereals such as wheat produce xylanase-inhibitory proteins in response to fungal infection (Chmelová *et al.*, 2019). Thus, the structural complexity of xylan, and its effects on xylan digestibility may have important effects during infection by pathogens.

In this work, we identified the glycosyltransferases responsible for decorating xylan GlcA residues in both Arabidopsis and *Eucalyptus grandis*. Using a synthetic biology approach, we engineered Arabidopsis SCW xylan so that the majority of its GlcA branches exhibited Ara*p* or Gal substitutions. These highly substituted novel xylans may have useful biotechnological properties, and may affect cell wall degradation by plant pathogens. We demonstrate the difference in tissue distribution between $U^{Ara\mathit{p}}$ and U^{Gal} structures in *Eucalyptus* spp., and, by analysing the evolution of the GT47-A_V family (Yu *et al.*, 2022), explain how the U^{Gal} structure has arisen specifically within the Myrtaceae family. Furthermore, we show not only that the decoration of GlcA with Ara*p*/Gal impedes the action of some GH30 glucuronoxylanases, but also that a convergently acquired amino acid substitution allows others to accommodate such structures. As well as providing insight into the synthesis and function of PCW xylan and the arms race between plants and pathogens, our results could therefore help increase efficiency in industrial hemicellulosic biomass degradation.

Materials and Methods

Plant Material

All Arabidopsis (*Arabidopsis thaliana* (L.) Heynh.) T-DNA insertion mutant lines were in the Col-0 ecotype. *At1g68470* (*Atgt17/xapt1*): WiscDsLox437H04 (*xapt1-1*), *at2g29040* (*Atgt11*): Salk_108349, *at2g32750* (*Atgt12*): Salk_057536, *at2g32740* (*Atgt13*): Salk_053593C, *at4g22580* (*Atgt19*): Salk_075020 and *at5g41250*: Salk_085915 (*Atgt20*) were obtained from the Nottingham Arabidopsis Stock Centre (NASC, Nottingham, UK). Homozygous lines were isolated by PCR. The *irx9l* (SALK_037323) and *mur3-3* mutants have been described previously (Wu *et al.*, 2010; *Kong et al.*, 2015). All the primers used are shown on Table S1. Arabidopsis young stem was harvested at 30 days and bottom stem was harvested at 8 weeks.

Actively growing *Eucalyptus dalrympleana* Maiden branch and leaves were harvested at Jesus College, University of Cambridge in April 2018. Young, actively growing *Myrtus communis* L. and *Metrosideros excelsa* Sol. ex Gaertn. branchlets were harvested at Cambridge University Botanic Garden, and *Plinia cauliflora* (Mart.) Kausel, *Psidium guajava* L., and *Myrcianthes pungens* (O.Berg) D.Legrand material was a gift of Pedro Araújo (University of Campinas). Combined phloem and periderm cortex material was separated from xylem/pith by peeling or scraping. After collection, all the materials were put into 96% ethanol. For all samples, alcohol insoluble residue (AIR) was prepared as described previously (Goubet *et al.*, 2009).

Plant Growth and Arabidopsis transformation

Arabidopsis plants were grown on a 9:1 mix of Levington M3 compost and vermiculite and grown at 21°C under a 16 h/8 h photoperiod. Constructs used for *A. thaliana* Xylan ArabinoPyranosylTransferase 1 (*At*XAPT1), *Eucalyptus grandis* W.Hill ex Maiden (*Eg*XAPT), and Xylan GalactoPyranosylTransferase (*Eg*XLPT) overexpression in *xapt1* and WT plants were prepared using OpenPlant common syntax GoldenGate assembly (Patron *et al.*, 2015). *AtXAPT1* (*At1g68470*), *EgXAPT* (*Eucgr.D00738*; GenBank: XM_010054097.3), and *EgXLPT* (*Eucgr.H00343*; GenBank: XM_010070979.3) coding sequences and the *CESA3* and *IRX3* promoter sequences were synthesised *de novo* by IDT or GeneWiz after removal of

BsaI and *BpiI* restriction sites. Arabidopsis transformation was performed using the floral dip method as previously described (Clough & Bent, 1998).

Phylogenetic and bioinformatics analysis

For the XAPT phylogeny, XAPT orthologues from a wide range of tracheophyte species were extracted from our recent phylogeny of GT47-A enzymes (Yu *et al.*, 2022), which contained protein sequences from Plaza Dicots 4.5, Plaza Monocots 4.5, and Plaza Gymnosperms 1.0 (Van Bel *et al.*, 2018), as well as from several independent genomes. To obtain further XAPT orthologues from plants in the Myrtales order, the genomes of *Metrosideros polymorpha* (Izuno et al., 2016; Izuno et al., 2019), *Rhodamnia argantea*, *Syzygium oleosum*, and *Punica granatum* (all available from NCBI Genome, https://www.ncbi.nlm.nih.gov/genome/) and the transcriptome of *Oenothera rosea* (Carpenter et al., 2019; One Thousand Plant Transcriptomes, 2019), were searched using TBLASTN (Altschul *et al.*, 1990) using *At*XAPT1 as a query with a cut-off at $E = 1 \times 10^{-125}$. Sequences were aligned using MUSCLE (Edgar, 2004a; Edgar, 2004b) and truncated to the GT47 domain. ProtTest3 (Darriba *et al.*, 2011) was then used to select an appropriate substitution model, and a phylogeny was calculated using RAxML (Stamatakis, 2014) with 100 rapid bootstraps. For the main text figure, the tree was then trimmed to species of interest using ape 5.0 (Paradis & Schliep, 2019).

For the GH30 subfamily 8 tree, CAZy sequences were downloaded from the dbCAN2 server (http://bcb.unl.edu/dbCAN2/) (Zhang *et al.*, 2018). Using bespoke Python scripts invoking HMMER (Eddy, 2011), GH30_8 domain-containing sequences were extracted and trimmed to the GH30 domain. Sequences with a GH30 domain sequence shorter than 200 residues were omitted. Extremely similar sequences were removed using CD-HIT (Li & Godzik, 2006; Fu *et al.*, 2012) with a 99 % similarity threshold. The remaining sequences were aligned using MAFFT (Katoh & Standley, 2013); ProtTest3 was then used to select an appropriate substitution model, and a phylogeny was calculated using RAxML with 100 rapid bootstraps.

Genomic DNA extraction and sequencing of native *XAPT* and *XLPT* loci

E. dalrympleana leaves were ground in liquid nitrogen and genomic DNA was extracted as previously described (James *et al.*, 2001), supplementing the extraction buffer with 3 % polyvinylpyrrolidone. PCR amplification was achieved using Q5 High-Fidelity DNA Polymerase (New England Biolabs, Ipswich, MA, USA) according to manufacturer's instructions. Primers are listed in Table S1. PCR products were purified by gel extraction and isopropanol precipitation before Sanger sequencing by the DNA Sequencing Facility of the Department of Biochemistry, University of Cambridge.

Enzyme Digestions

Soluble hemicelluloses were prepared from AIR as previously described (Lyczakowski *et al.*, 2017). For Arabidopsis bottom stem and *E. dalrympleana* xylan analysis, 0.5 mg AIR was used for one reaction. For Arabidopsis young stem, 1 mg AIR was used for one reaction.

Soluble hemicellulose fraction was digested with an excess of Xyn11A from *Neocallimastix patriciarum* (*Np*Xyn11A, Genbank: CAA46498.1; from Megazyme, Ireland) in 50 mM ammonium acetate, pH 6.0 at 30°C overnight.

Alternatively, xylan was digested with GH30 xylanases with a 70 μg ml^{-1} concentration from different bacteria at 25°C for 30 min in 50 mM ammonium acetate, pH 6.0. The GH30 xylanases included: XynC from *Bacteroides ovatus (Bo*XynC, GenBank: ALJ48333.1; a gift of Harry Gilbert, Newcastle University); Xyn30A from *Hungateiclostridium thermocellum* (*Ct*Xyn30A, GenBank: ABN54208.1; from NZYTech, Portugal). XynA from *Dickeya chrysanthemi* strain D1 (Ec_{D}Xyn30A, GenBank: AAB53151.1), XynA from *Dickeya chrysanthemi* strain P860219 (Ec_{P}Xyn30A, GenBank: AAL16415.1), and the two mutagenized enzymes Ec_{D}Xyn30A$_{Y255L}$ and Ec_{P}Xyn30A$_{L255Y}$ were provided by Novozymes A/S (Bagsværd, Denmark). For mass spectrometry and galactosidase sensitivity experiments, xylanase products were then digested overnight with 10 μL of 1 mg ml^{-1} *B. ovatus* GH115 glucuronidase (*Bo*Agu115A, GenBank: EDO10816.1; a gift of Harry Gilbert, Newcastle University) to remove the non-decorated GlcA side chains.

For the galactosidase sensitivity assay, the xylanase products were passed through a 3 kDa Nanosep centrifugal device. Next, ethanol was added to a final concentration to 65% before incubation at −20°C for 2 h. The samples were then centrifuged at 12,000g for 10 min; the

supernatant was subsequently dried 60°C *in vacuo* and resuspended in 200 µl of 50 mM ammonium acetate, pH 6.0. To this, 0.5 µl of 4 kU ml^{-1} GH35 β-galactosidase from *Aspergillus niger* (Megazyme, Ireland) was added and incubated at 37°C for 18 h. Samples were then dried at 60°C *in vacuo*.

Oligosaccharides Fingerprint Analysis by PACE

Samples and $(Xyl)_{1–6}$ standards (Megazyme, Ireland) were derivatized with 8-aminonapthalene-1,3,6-tresulphonic acid (ANTS; Invitrogen) as described previously (Goubet et al., 2002). After drying, the samples were resuspended in 100 µl of 3 M urea (final concentration of standards = 20 µM), of which 2 µl was loaded onto the PACE gels. The samples were run and visualized as described previously (Goubet *et al.*, 2009).

Preparation of Oligosaccharides for MS

Following the enzyme digestion, released peptides and enzymes were removed using reverse-phase Sep-Pak C18 cartridges (Waters, MA, USA) as previously described. Oligosaccharides were reductively aminated with 2-aminobenzoic acid (2-AA), using optimized labelling conditions as previously described (Tryfona & Stephens, 2010). The labelled samples were then purified from reductive amination reagents using a GlycoClean S cartridge (ProZyme, CA, USA) as described previously (Tryfona *et al.*, 2010).

Results

At1g68470 encodes *XYLAN ARABINOPYRANOSYLTRANSFERASE 1* (*XAPT1*) in Arabidopsis

We recently established that PCW xyloglucan and β-galactoglucomannan (β-GGM) polysaccharides in Arabidopsis have significant similarities in their structure and biosynthesis (Yu *et al.*, 2022). In particular, both polysaccharides exhibit β1,2-galactosylation of their α1,6-linked backbone decorations (to produce Gal-β1,2-Xyl-α1,6- and Gal-β1,2-Gal-α1,6-side chains, respectively). By comparison with previously identified xyloglucan galactosyltransferases from the GT47-A glycosyltransferase family, MUR3 and XLT2, we successfully predicted that the equivalent galactosyltransferase for β-GGM, MBGT1, would

reside in the same family. Since verifying the activity of MBGT1, we were curious to see whether other GT47-A members might work on further polysaccharides. Seeing as α-L-Ara*p* differs from β-D-Gal by only a hydroxymethyl group, we hypothesised that α1,2-arabinopyranosylation of PCW xylan glucuronic acid decorations (Ara*p*-α1,2-GlcA-α1,2-) might also be mediated by a member of this family.

To test this hypothesis, we attempted to detect the loss of the PCW xylan U^{Arap} structure in T-DNA knockout lines for the six remaining GT47-A subclade members with unknown functions (*At2g29040/AtGT11*, *At2g32750/AtGT12*, *At2g32740/AtGT13*, *At1g68470/AtGT17*, *At4g22580/AtGT19*, and *At5g41250/AtGT20*). *At2g29040*/*AtGT11* has since been implicated in galactosylation of pollen tube xyloglucan (Wei *et al.*, 2021). We used the *irx9l* mutant, which lacks PCW-type xylan (and therefore does not exhibit any U^{Arap} structure), as a control (Mortimer *et al.*, 2015). AIR from the young stems of these mutants was incubated with alkali to solubilize the hemicelluloses, and then digested with *Np*Xyn11A *endo*-xylanase. The resultant oligosaccharides were analysed by PACE. As previously reported (Mortimer *et al.*, 2015), wild-type (WT) young stem yielded a series of products including xylose (X), xylobiose (X_2), aldopentaouronic acid with ($XU^{m}XX$) or without (XUXX) 4-O-methyl group on the GlcA (generically termed '$XU^{[m]}XX$'), and xylopentaose substituted with the putative Ara*p*-GlcA- disaccharide ($XU^{Arap}XXX$). In contrast, digestion of material from the *irx9l* mutant released xylose, xylobiose (X_2), and $XU^{[m]}XX$, but not $XU^{Arap}XXX$. Interestingly, although we could detect $XU^{Arap}XXX$ in five of the six GT47-A mutants, this product was also conspicuously absent for *at1g68470*, suggesting that xylan in this mutant lacks the U^{Arap} decoration (Fig. 1a, S1). To help confirm this, WT young stem was hydrolysed with the GH30-family xylanase Xyn30A from *Bacteroides ovatus* (*Bo*XynC), which requires a GlcA substitution at its −2 subsite. As previously described (Mortimer *et al.*, 2015), digestion of WT material with *Bo*XynC produced $XXXXU^{[m]}X$ ($U_1^{[m]}X_6$) and $XXXXU^{Arap}X$ ($U_1^{Arap}X_6$) as major products, in accordance with the consistent GlcA spacing of PCW xylan. In contrast, digestion of material from the *at1g68470* mutant released $U_1^{[m]}X_6$ but not the $U_1^{Arap}X_6$ oligosaccharide (Fig. 1b). These results suggest that *At1g68470* is required for the synthesis of the putative Ara*p*-GlcA- disaccharide substitution on Arabidopsis PCW xylan.

To further support our conclusion, we complemented the *at1g68470* mutant with *At1g68470* under the control of the PCW-synthesis-specific *CESA3* promoter. AIR from young stems was digested by xylanase *Np*Xyn11A and analysed by PACE. In all three independent

transgenic lines, the XU$^{Ara\mathit{p}}$XXX product was detected at substantially higher levels than in WT (Fig. 1a). Based on these data, and the previous arabinopyranose assignment, we concluded that *At1g68470* likely encodes a xylan-specific arabinopyranosyltransferase that catalyses the formation of an Ara*p*-α1,2-GlcA linkage. We therefore propose that *At1g68470* is named ***X**YLAN **A**RABINO**P**YRANOSYL**T**RANSFERASE 1* (*XAPT1*).

xapt1 **mutant plants do not exhibit a growth phenotype**

We investigated the importance of U$^{Ara\mathit{p}}$ disaccharide substitutions on Arabidopsis PCW xylan for plant growth through observation of the *xapt1* growth phenotype. *xapt1* plants grew similarly to WT plants and exhibited no obvious morphological differences (Fig. S2). However, since XAPT1 activity is similar to that of xyloglucan β-galactosyltransferase MUR3, we reasoned that there could be some functional redundancy between the two enzymes, as we recently showed for MUR3 and its paralogue glucomannan β-galactosyltransferase MBGT1 (Yu *et al.*, 2022). Hence, we crossed *xapt1* with the *mur3-3* mutant to produce double mutant plants. Nevertheless, there was no clear difference in the growth of the *xapt1 mur3-3* double mutant and the *mur3-3* single mutant. Hence, XAPT1 function does not appear to have a clear role in plant growth.

XAPT underwent gene duplication in the Myrtales

Whereas the U$^{Ara\mathit{p}}$ xylan branch structure has been reported in a wide range of species, including Arabidopsis, *Eucalyptus* spp., and non-commelinid monocots, the U^{Gal} structure has so far only been detected in *Eucalyptus* spp. (Togashi *et al.*, 2009; Pena *et al.*, 2016). Hence, we were interested to know if *Eucalyptus* spp. possess a unique galactosyltransferase responsible for these decorations. In our previous study, we showed that within GT47-A, XAPT1 belongs to a distinct subclade from xyloglucan- (MUR3, XLT2, XUT1) and β-GGM-modifying (MBGT) enzymes (Yu *et al.*, 2022). This putative XAPT subclade (GT47-A_V) contains representatives from Selaginella, gymnosperms, dicots, and non-Poaceae monocots. Because the U$^{Ara\mathit{p}}$ and U^{Gal} decorations are highly similar in structure (with Ara*p* lacking only the C6 hydroxymethyl group of Gal), we hypothesised that the galactosyltransferase responsible for U^{Gal} side chains might belong to the same subclade. To explore this idea, we constructed a phylogeny of XAPT homologues from 56 species of vascular plant, including *Eucalyptus grandis*, three fellow members of the Myrtaceae family (*Metrosideros*

polymorpha, *Syzygium oleosum*, and *Rhodamnia argantea*), and two members of the wider Myrtales order (*Punica granatum* and *Oenothera rosea*). Fig. 2 presents the rooted phylogeny, which has been trimmed for brevity (the full phylogeny can be found in Fig. S3). We found that most of the plant genomes—including *P. granatum* and *O. rosea*—exhibited a single gene in this subclade. In contrast, all four Myrtaceae genomes exhibited two paralogues that appear to have arisen from a single, recent duplication event in the Myrtales order. In the case of *E. grandis*, these two paralogues correspond to the genes *Eucgr.D00738* and *Eucgr.H00343*. Hence, we hypothesised that Eucgr.D00738 (*Eg*XAPT, hereafter) and Eucgr.H00343 (*Eg*XLPT) could each constitute either a xylan GlcA arabinopyranosyltransferase or potentially a xylan GlcA galactosyltransferase.

Eucgr.D00738 **and** ***Eucgr.H00343*** **encode** ***Eg*****XAPT and** ***Eg*****XLPT**

To investigate the activities of the two Myrtaceae XAPT-related paralogues in GT47-A, we expressed *Eg*XAPT and *Eg*XLPT under the strong, PCW-synthesis-specific *CESA3* promoter in the *xapt1* mutant. Xylan digestion with *Np*Xyn11A xylanase revealed that disaccharide side chain structures were restored in the young stems of two transgenic lines for each construct (Fig. 3a), suggesting that both proteins are active and catalyse the formation of Ara*p*-α1,2-GlcA or a similar linkage on xylan.

PCW xylan is the presumed natural substrate of XAPT in Arabidopsis, but PCW xylan scarcity *in planta* makes its structure difficult to analyse. For this reason, we expressed the two *E. grandis* enzymes in SCW-producing tissues, which synthesise much more xylan. Furthermore, $^{[Me]}$GlcA sidechains on SCW xylan are completely unsubstituted (Bromley *et al.*, 2013; Mortimer *et al.*, 2015), which produces an ideal background for characterisation of *Eg*XAPT and *Eg*XLPT. The *Eg*XAPT and *Eg*XLPT coding sequences were placed under the control of the SCW-synthesis-specific *IRX3* promoter and expressed in WT Arabidopsis, and xylan from mature bottom-stems was digested with the glucuronoxylanase *Bo*XynC and analysed by PACE. As described previously (Bromley *et al.*, 2013), digestion of the WT xylan released products decorated with unsubstituted GlcA ($U_1^{[m]}X_n$), whose sizes corresponded to expected $^{[Me]}$GlcA spacings (Fig. 3b). In the *Eg*XAPT- and *Eg*XLPT-expressing lines, however, similar analysis revealed very different oligosaccharide products, suggesting that most of the $^{[Me]}$GlcA had been modified, perhaps into $U^{Ara\mathit{p}/Gal,[m]}$ structures. The spacing between GlcA decorations along the xylan backbone did not appear to be

affected in these transgenic plants. Interestingly, oligosaccharides with substituted GlcA in *Eg*XLPT-expressing lines migrated marginally slower than those in *Eg*XAPT-expressing lines, suggesting that the products of *Eg*XAPT and *Eg*XLPT might differ subtly in structure.

To further characterise the products of *Eg*XAPT and *Eg*XLPT, xylan from the relevant transgenic lines was digested simultaneously with *Np*Xyn11A and a *Bacteroides ovatus* GH115 (*Bo*GH115) α-glucuronidase, which removes unsubstituted GlcA side chains. As expected, PACE analysis indicated that WT bottom-stem xylan was fully digested into xylose and xylobiose (Fig. S4). In the *Eg*XAPT- and *Eg*XLPT-expressing lines, however, a band of higher molecular weight ($XU^{Arap,[m]}XXX/XU^{Gal,[m]}XXX$) was produced. To distinguish between any arabinopyranosylated and galactosylated oligosaccharides, we then treated these products with a β-galactosidase (*An*GH35). Whereas the higher-molecular-weight band from *Eg*XAPT-expressing lines was completely insensitive to *An*GH35 (revealing it to be entirely $XU^{Arap,[m]}XXX$), almost all of the equivalent product from *Eg*XLPT-expressing lines shifted to $XU^{[m]}XXX$ after β-galactosidase treatment—revealing its identity as $XU^{Gal,[m]}XXX$ and indicating the presence of the U^{Gal} structure in these plants. These results suggest that *Eg*XLPT, but not *Eg*XAPT, is capable of transferring galactose to GlcA side chains.

To confirm these assignments, we analysed *Bo*XynC glucuronoxylanase products by mass spectrometry (MS), which can distinguish between pentose and hexose substituents. To prevent further ambiguity between $U_1^{[m]}X_n$ and $U_1^{Arap,[m]}X_{n-1}$, *Bo*XynC products were treated with α-glucuronidase *Bo*GH115 to remove unsubstituted GlcA residues, thereby leaving $U_1^{Arap/Gal}X_n$ oligosaccharides as the only acidic products. The resulting oligosaccharides were derivatised with 2-aminobenzoic acid (2-AA) and then analysed by MALDI-TOF MS (Fig. 4, S5). As predicted, only xylo-oligosaccharides were produced from WT, confirming full removal of unsubstituted $^{[Me]}$GlcA by the α-glucuronidase. Products from plants expressing *At*XAPT under the same promoter were analysed in parallel for comparison. Lines expressing *At*XAPT and *Eg*XAPT exhibited abundant amounts of $U_1^{Arap}X_n$ and low amounts of $U_1^{Arap,m}X_n$, confirming that *Eg*XAPT is a xylan arabinopyranosyltransferase. In lines expressing *Eg*XLPT, however, the dominant sugars released could be assigned as $U_1^{Gal}X_n$, with a smaller presence of $U_1^{Gal,m}X_n$. Interestingly, this approach also detected low amounts of $U_1^{Arap}X_n$ and $U_1^{Arap,m}X_n$ in all *Eg*XLPT independent lines (Fig. 4, S5). These results suggest that *Eg*XLPT is primarily a xylan galactosyltransferase with a low level of arabinopyranosyltransferase activity, at least when expressed in Arabidopsis.

Different *Eucalyptus dalrympleana* tissues contain structurally distinct xylans

Although U^{Arap} and U^{Gal} side chains are known to exist in plants from the *Eucalyptus* genus (Togashi *et al.*, 2009; Pena *et al.*, 2016), the tissue distribution of these structures is unknown, limiting our insight into their function. To investigate where the enzymes might be active, we studied expression data available for *EgXAPT* and *EgXLPT* at https://EucGenIE.org (Hefer et al., 2011), which provides mRNA-Seq datasets for both *E. grandis* and the hybrid *E. grandis* × *E. urophylla*. Despite some potential disagreement between the two datasets, a clear pattern was still apparent: whereas *EgXAPT* expression is relatively constant and lowest in xylem tissues, the expression of *EgXLPT* is much stronger in xylem tissues than in leaves, flowers, and shoot tips (Fig. S6, S7). Interestingly, the expression of *EgXLPT* is dramatically higher in *E. grandis* × *E. urophylla* tension wood xylem than control xylem, as has been previously noted (Mizrachi *et al.*, 2015).

To study the predicted xylan structure distributions *in planta*, we harvested an actively growing branch of *Eucalyptus dalrympleana* (mountain gum). To confirm that the *XAPT* and *XLPT* genes of *E. dalrympleana* do not differ substantially to those of *E. grandis*, we PCR-amplified them from genomic DNA using homology-based primers and sequenced the two intronless coding sequences, revealing 98% (XAPT) and 99% (XLPT) protein identity between the *E. dalrympleana* and *E. grandis* sequences (Fig. S8, S9). Next, to determine the extent of GlcA substitution amongst *E. dalrympleana* tissues, we sectioned the branch into cortex, phloem, sapwood/xylem, and leaf. Major leaf veins were removed to avoid contamination from vascular tissue (Fig. 5a). Alkali-treated AIR from each tissue was digested with *Bo*XynC xylanase and analysed with PACE. Based on the PACE xylo-oligosaccharide profiles, the tissues broadly fell into two groups with very different xylan structures (Fig. 5b). In the first group, which comprises leaf and phloem, $U_1^{[m]}X_6$ and $U_1^{Arap/Gal,[m]}X_6$ were the most abundant xylan oligosaccharides, with traces of $U_1^{[m]}X_5$ and $U_1^{Arap/Gal,[m]}X_5$. In the other group, which comprises cortex and xylem, the oligosaccharides were dominated by xylo-oligosaccharides decorated with single $^{[Me]}$GlcA. The cortex and xylem xylan had a GlcA spacing pattern very similar to SCW xylan from Arabidopsis (Bromley *et al.*, 2013). Small amounts of $U_1^{Arap/Gal,[m]}X_5$ and $U_1^{Arap/Gal,[m]}X_6$ oligosaccharide could also be detected in cortex and xylem.

In order to discriminate U^{Arap} and U^{Gal} structures in different Eucalyptus tissues, we again treated *Bo*XynC xylanase products with α-glucuronidase GH115 and analysed the remaining

acidic products by MS. The MS profile of xylan showed that neutral and acidic oligosaccharides were released from all tissues but with different ratios (Fig. 6). Consistent with the expression data (Fig. S6, S7), leaf tissue released $U_1^{Arap,m}X_5$ and $U_1^{Arap,m}X_6$ oligosaccharides but no $U_1^{Gal,m}X_n$ oligosaccharides. In contrast, the stem tissues yielded detectable levels of $U_1^{Gal,m}X_5$ and $U_1^{Gal,m}X_6$. From cortex to phloem to xylem, the percentage of GlcA residues that were substituted decreased, while at the same time, the ratio of Gal to Ara*p* decorations increased. We did not detect any structures containing unmethylated GlcA. In summary, both the patterning and substitution of xylan GlcA side chains varies in different *E. dalrympleana* tissues and appears to correspond with the previously observed expression patterns of *Eg*XAPT and *Eg*XLPT in *E. grandis* / *E. grandis x E. urophylla*. More specifically, XAPT appears to be responsible for arabinosylating glucuronoxylan mainly in certain PCW-rich tissues, whereas glucuronoxylan galactosylation by XLPT appears to be enriched in woody tissues but is less abundant overall.

Other Myrtaceae plants contain U^{Gal} and U^{Arap} structures in their xylan

The results of our phylogenetic analysis suggested that other genera in the Myrtaceae family might possess XLPT orthologues, and therefore might exhibit U^{Gal} structures on their xylan. To investigate this hypothesis, we sectioned and analysed tissue from five additional Myrtaceae members: *Myrtus communis* (myrtle), *Metrosideros excelsa* (pohutukawa), *Plinia cauliflora* (jaboticaba), *Psidium guajava* (guava), and *Myrcianthes pungens* (guabiju). Xylan extracted from both cortex/phloem (combined) and xylem/pith was treated with xylanase *Np*Xyn11A and α-glucuronidase *Bo*GH115, and as before, the products were subsequently digested with *An*GH35 β-galactosidase. In xylem/pith, $XU^{Arap,[m]}XXX/XU^{Gal,[m]}XXX$ oligosaccharides were detectable in all species, with *M. communis* exhibiting remarkably high levels of GlcA substitution (Fig. S10). Notably, for *M. communis*, *P. cauliflora*, *P. guajava*, and *M. pungens* xylan, but not *M. excelsa*, a large proportion of this $XU^{Arap,[m]}XXX/XU^{Gal,[m]}XXX$ product was sensitive to *An*GH35, indicating that this band was primarily composed of the $XU^{Gal,[m]}XXX$ oligosaccharide with a smaller amount of $XU^{Arap}XXX$ in xylem (Fig. S10). In cortex/phloem, $XU^{Arap,[m]}XXX/XU^{Gal,[m]}XXX$ oligosaccharides were detectable in all species except in *P. cauliflora* (Fig. S11). However, only *M. communis* yielded products that were sensitive to *An*GH35, suggesting a lack of $U^{Gal,[m]}$ structures in the cortex/phloem of the other four species. Our results therefore support

the idea that many Myrtaceae plants exhibit U^{Gal} side chains and that this structure is enriched in woodier tissues.

GH30-family glucuronoxylanases have convergently evolved to overcome the obstacle of glucuronyl side chain modification

Cell wall polysaccharides constitute a barrier to potential pathogens. Plant pathogens therefore rely on polysaccharide-degrading enzymes for their virulence. In this work, we have used two *endo*-xylanases to analyse xylan structure: *Np*Xyn11A, from CAZy family GH11, and *Bo*XynC, a member of GH30 subfamily 8 from the gut bacterium *B. ovatus*. In order to act on xylan, the latter of these specifically recognises and binds to GlcA substitutions. Curiously, previously solved crystal structures of related GH30 xylanases from plant pathogen *Dickeya chrysanthemi* (previously *Erwinia chrysanthemi*) strain D1 (Ec_{D}Xyn30A) and *Bacillus subtilis* (*Bs*XynC) show that both enzymes make a hydrogen bond to the C2 hydroxyl of GlcA using the phenol group of Tyr_{255} or Tyr_{231} respectively (Fig. 7a) (St John *et al.*, 2011; Urbanikova *et al.*, 2011). We reasoned that the 1,2-linked Ara*p*/Gal substitution that decorates GlcA residues at this very hydroxyl should therefore impede Ec_{D}Xyn30A and *Bs*XynC from binding their substrate. In spite of this, our results clearly showed that the related *Bo*XynC is able to bind and cleave at the $U^{Arap/Gal}$ decorations (Figs. 1b, 3b). To determine whether Ec_{D}Xyn30A and other GH30 xylanases might have the same activity, we digested xylan from Arabidopsis *gux1,2* young stem with Ec_{D}Xyn30A or *Ct*Xyn30A (from *Clostridium thermocellum*). PACE analysis of the products revealed that, whereas *Bo*XynC is capable of cleaving the xylan backbone adjacent to both substituted and unsubstituted $^{[Me]}$GlcA, Ec_{D}Xyn30A and *Ct*Xyn30A are only able to cleave effectively at unsubstituted $^{[Me]}$GlcA decorations (Fig. 8a). These results demonstrate a hitherto unknown substrate specificity variant amongst GH30 glucuronoxylanases.

To help understand the difference in substrate specificity between these enzymes, we aligned their protein sequences. The alignment showed that the tyrosine residue involved in binding the C2 hydroxyl of GlcA is also present in *Ct*Xyn30A. Interestingly, however, the corresponding residue in *Bo*XynC is not tyrosine but leucine (Fig. 7b).

To investigate the extent of amino acid variety at this position, we conducted a phylogenetic analysis of the entire GH30 subfamily 8. We then labelled the sequences in the tree according to the amino acid at the position of interest. The results showed that *Bo*XynC belongs to a

distinct subgroup of enzymes with leucine rather than tyrosine at this position (Fig. 7c). Interestingly, we also identified an enzyme from *D. chrysanthemi* P860219 that diverged much more recently from *Ec*$_{D}$Xyn30A than *Bo*XynC, but has independently acquired a leucine at this position (we henceforth refer to this enzyme as *Ec*$_{P}$Xyn30A) (Fig. 7b, c). Although *Ec*$_{D}$Xyn30A and *Ec*$_{P}$Xyn30A otherwise share 82% protein sequence identity, like *Bo*XynC, *Ec*$_{P}$Xyn30A (but not *Ec*$_{D}$Xyn30A) was able to cut xylan adjacent to U$^{Ara\mathit{p}/Gal}$ decorations (Fig. 8b).

To investigate whether this single residue difference is sufficient to explain the discrepancy in substrate specificity, we performed site-directed mutagenesis on the *Ec*$_{D}$Xyn30A and *Ec*$_{P}$Xyn30A enzymes. Leu$_{255}$ from *Ec*$_{P}$Xyn30A was mutated to tyrosine to produce *Ec*$_{P}$Xyn30A$_{L255Y}$, while Tyr$_{255}$ from *Ec*$_{D}$Xyn30A was mutated to leucine to produce *Ec*$_{D}$Xyn30A$_{Y255L}$. Initially, we used the purified enzymes to digest WT bottom-stem xylan without Ara*p*/Gal substitutions. All four enzymes released identical products of the same quantities, suggesting that all four variants exhibit glucuronoxylanase activity (Fig. S12). We used the purified enzymes to hydrolyse alkali-extracted xylan from plants expressing the $_{pro}$*IRX3*:*EgXLPT*/*XAPT* constructs. As predicted, both *Ec*$_{D}$Xyn30A and *Ec*$_{P}$Xyn30A$_{L255Y}$ produced primarily xylo-oligosaccharides with GlcA residues, whereas the enzymes *Ec*$_{P}$Xyn30A and *Ec*$_{D}$Xyn30A$_{Y255L}$ could release many more products with U$^{Ara\mathit{p}/Gal}$ decorations (Fig. 8b). These data suggest that a tyrosine residue at this position prevents efficient activity on xylan substrates with substituted GlcA decorations (or that leucine is required at this position for activity), and that multiple GH30 glucuronoxylanase subfamilies have independently adapted to accommodate substituted GlcA decorations.

Discussion

In this work, we have identified the enzymes responsible for decorating GlcA xylan side branches in Arabidopsis and *Eucalyptus* spp.. All three enzymes belong to subclade V of the GT47-A family (Yu *et al.*, 2022). Interestingly, all known activities from this family involve the formation of a 1,2 glycosidic bond between the donor sugar and an α-linked backbone substitution of a hemicellulose. Furthermore, XAPT1 is the third GT47-family enzyme found to be involved in xylan synthesis, with IRX10 and XYS1/IRX10L already belonging to GT47-D (Li *et al.*, 2004; Brown *et al.*, 2009).

The identity of the pentosyl residue decorating GlcA branches in Arabidopsis PCW xylan has not been fully confirmed: previous attempts to identify it by NMR could not distinguish between α1,2-linked arabinopyranose and β1,2-linked xylose. Nevertheless, the former is favoured because the decoration is insensitive to β-xylosidase (Mortimer *et al.*, 2015). Furthermore, the equivalent pentosyl decorations in *Eucalyptus grandis* and non-commelinid monocots have been unambiguously determined to be α1,2-linked arabinopyranose (Pena *et al.*, 2016). The close evolutionary relationship between the Arabidopsis and *E. grandis* XAPT enzymes further strengthens the idea that the Arabidopsis pentosyl decoration is indeed arabinopyranose. Hence, we are confident in assigning *At*XAPT1 as an arabinopyranosyltransferase.

The identification of XAPT and XLPT enzymes in GT47-A_V helps to explain the distribution of substituted GlcA xylan side chains amongst plant species. Our previous phylogeny (Yu *et al.*, 2022) demonstrated that GT47-A_V genes have been completely lost from grass (Poaceae) genomes. This explains why U^{Arap} side chains have been observed in non-commelinid monocot orders (Asparagales, for instance), but never in grasses. Traditionally, a distinction has been made between commelinid and non-commelinid plants in terms of their cell wall structures; however, our phylogeny shows that even some members of the commelinid Poales order (*Ananas comosus*, for example) exhibit a XAPT orthologue. In addition, our work explains the emergence of U^{Gal} side chains in the Myrtaceae family. We conclude that such structures arose from a recent duplication and neofunctionalisation of the *XAPT* locus in a subgroup of the Myrtales or Myrtaceae. Whether galactosyl decorations have any functional distinction from arabinopyranosyl decorations is unclear, especially as we did not observe a difference in preference between the two by any GH30 glucuronoxylanase. It is possible that the difference in sugar substitution could have consequences for the action of individual *exo*-glycosidases—be they microbial or cell wall remodelling enzymes (such as the β-galactosidase MUM2).

Unlike arabinoxylan, glucuronoxylan is present to at least some extent in virtually every land plant cell wall. Therefore, the properties of GlcA may have a specific and important role in cell wall structure. For instance, in secondary cell walls, GlcA has been reported to form the covalent bridge to lignin polymers *via* its C6 carboxylate (Giummarella *et al.*, 2019; Terrett & Dupree, 2019). The GlcA may also be important, alongside acetylation, for xylan solubility and assembly onto cellulose (Schultink *et al.*, 2015). Further modification of GlcA by 2-*O*-

arabinopyranosylation, 2-*O*-galactosylation, and/or 4-*O*-methylation could therefore potentially modulate xylan incorporation into the cell wall. At the same time, the $U^{Ara\mathit{p}}$ and U^{Gal} disaccharide side chains resemble the functionally important side chains of other PCW hemicelluloses: namely, the Gal-β1,2-Xyl-α1,6- and Gal-β1,2-Gal-α1,6- side chains of xyloglucan and β-GGM, respectively. Computational studies of xyloglucan oligosaccharides have suggested that the β1,2-linked galactosyl residues interact with the polysaccharide backbone and weaken its binding to cellulose microfibrils (Zhao *et al.*, 2014). The galactosyl residues may also influence xyloglucan solubility during biosynthesis (Tamura *et al.*, 2005; Kong *et al.*, 2015). Whether decoration of GlcA could have an effect on xylan–cellulose interactions will require extensive computational and solid state NMR work to establish.

Despite these possibilities, but consistent with GlcA methyltransferase mutants (Urbanowicz *et al.*, 2012; Li *et al.*, 2013) and glucuronyltransferase mutants (Mortimer *et al.*, 2015), we did not observe any obvious phenotype of *xapt* or *xapt mur3-3* plants, which fails to support an important function for such decorations in normal plant growth. Nevertheless, we observed an interesting interplay between the two types of GlcA modification: whereas all GlcA residues in the *E. dalrympleana* disaccharide side chains were methylated, the equivalent GlcA residues in our *Eg*XAPT and *Eg*XLPT transgenic Arabidopsis lines were almost completely unmethylated. This might suggest that Arabidopsis GlcA 4-*O*-methyltransferases do not accept substituted GlcA residues. Furthermore, some clues for the function of $U^{Ara\mathit{p}}$ and U^{Gal} structures may lie in their uneven tissue distribution. Based on previous comparisons between 'young' and 'old' stems in Arabidopsis, $U^{Ara\mathit{p}}$ structures have so far been assumed to be a general feature of 'PCW xylan' (Mortimer *et al.*, 2015). However, in the Myrtaceae family at least, we have shown that the distribution of decorations is likely to be more complicated than that. For example, while $U^{Ara\mathit{p}}$ structures could be found in typically PCW-rich organs and tissues such as leaf, cortex, and phloem, U^{Gal} structures were specifically enriched in xylem/pith but completely absent from leaves. Furthermore, given that our dissections lacked the precision to separate individual cell types, it is possible that substitution of GlcA is limited to specialised cells within the tissues of interest. Single-cell expression atlases for Arabidopsis stem (Shi *et al.*, 2021) and leaf (Kim *et al.*, 2021) lend support to this idea by suggesting that *At*XAPT expression may be selectively enriched in cell types such as cambium, phloem parenchyma, and/or stem epidermis. Moreover, although we did not investigate the xylan structures *in planta*, *Eg*XLPT appears to be specifically upregulated in tension wood xylem tissues—perhaps by as much as a 50-fold increase

(Mizrachi *et al.*, 2015)—hinting at a specific structural role in the cell wall. As previously proposed, it is possible that xylan structure could be remodelled in tension wood, perhaps in a way that affects its incorporation into the wall.

Whether or not the GlcA branches on xylan play a structural role in the cell wall, their absence leads to a major reduction in biomass resistance to enzymatic saccharification (Lyczakowski *et al.*, 2017), suggesting that they may constitute a direct or indirect factor in plant-pathogen interaction. Here, we have uncovered that the substitution of GlcA residues likely affects the ability of GH30-family glucuronoxylanases to degrade xylan. Remarkably, different lineages of this family appear to have convergently overcome the obstacle posed by C2 modification through a single point mutation. Interestingly, the strain of *D. chrysanthemi* whose glucuronoxylanase has recently acquired tolerance for these decorations, P860219, was apparently cultured from *Anthurium* sp.: a non-commelinid from the Alismatales order whose close relatives exhibit abundant U^{Arap} xylan side chains (Hurlbert & Preston, 2001). This is in contrast to substitution-intolerant strain D1, which was cultured from corn (Vroemen *et al.*, 1995), a member of the Poaceae that lacks any substitutions. This hints that cell wall structures could be applying a direct selection pressure on xylanase evolution.

In summary, we have identified one of the missing components of xylan synthesis in higher plants. The identification of XAPT1 permits engineering of existing xylan polysaccharides using synthetic biology approaches. Furthermore, by revealing previously unknown substrate specificities in GH30 glucuronoxylanases, our results could facilitate optimisation of industrial lignocellulosic biomass degradation. These results hint at the constant evolutionary battle between plants and pathogens.

Acknowledgements and funding

We thank Paul Stearn (Jesus College, Cambridge), Ángela Cano and Sam Brockington (Cambridge University Botanic Garden), and Pedro Araújo (University of Campinas) for providing plant material.

This work was supported by the Leverhulme Trust Centre for Natural Material Innovation, the Biotechnology and Biological Sciences Research Council (BBSRC) of the UK as part of the OpenPlant Synthetic Biology Research Centre (Reference BB/L014130/1), The UKRI grant underwriting the ERC advanced grant (EVOCATE Function and evolution of plant cell

wall architecture for sustainable technologies. EP/X027120/1), Innovate UK, the Cambridge BBSRC-DTP Programme (Reference BB/J014540/1), a Novo Nordisk Foundation grant Oxymist (Grant Number NNF20OC0059697), and a BBSRC iCASE studentship (Reference BB/M015432/1).

Competing interests: K.B.R.M.K. is an employee of Novozymes, a major enzyme producing company. The remaining authors declare no conflict of interests.

Author contributions

LY conceived the original screen, designed the study, performed most polysaccharide analyses and plant transformations, and co-wrote the paper; LFLW conducted the phylogenetic analyses, contributed to the biochemical analysis, designed the xylanase point mutations, and co-wrote the paper; OMT carried out the molecular biology, conducted xylanase expression and purification, and co-wrote the paper; JWR identified differences in xylanase activities and supported the biochemical analysis and identification of Arabidopsis T-DNA insertion lines; JJL supported the biochemical analysis and molecular biology; XY made the double mutant; KBRMK contributed to the design and production of mutated xylanases; PD designed and supervised the study, interpreted data and co-wrote the paper.

Data Availability

The data that support the findings of this study are available in the main text and in the Supporting Information for this article. Sequences for newly identified *Eucalyptus dalrympleana* XAPT and XLPT will be deposited in GenBank after acceptance. All plant material descried in this manuscript is available on a reasonable request from the corresponding authors.

References

Altschul SF, Gish W, Miller W, Myers EW, Lipman DJ. 1990. Basic local alignment search tool. *Journal of Molecular Biology* **215**(3): 403-410.

Anders N, Wilson LFL, Sorieul M, Nikolovski N, Dupree P. 2022. β-1, 4-Xylan backbone synthesis in higher plants: How complex can it be? *Frontiers in Plant Science* **13**.

Bellincampi D, Cervone F, Lionetti V. 2014. Plant cell wall dynamics and wall-related susceptibility in plant–pathogen interactions. *Frontiers in Plant Science* **5**: 228.

Bromley JR, Busse-Wicher M, Tryfona T, Mortimer JC, Zhang ZN, Brown DM, Dupree P. 2013. GUX1 and GUX2 glucuronyltransferases decorate distinct domains of glucuronoxylan with different substitution patterns. *Plant Journal* **74**(3): 423-434.

Brown DM, Zhang Z, Stephens E, Dupree P, Turner SR. 2009. Characterization of IRX10 and IRX10-like reveals an essential role in glucuronoxylan biosynthesis in Arabidopsis. *Plant Journal* **57**(4): 732-746.

Burton RA, Gidley MJ, Fincher GB. 2010. Heterogeneity in the chemistry, structure and function of plant cell walls. *Nature Chemical Biology* **6**(10): 724-732.

Busse-Wicher M, Gomes TCF, Tryfona T, Nikolovski N, Stott K, Grantham NJ, Bolam DN, Skaf MS, Dupree P. 2014. The pattern of xylan acetylation suggests xylan may interact with cellulose microfibrils as a twofold helical screw in the secondary plant cell wall of Arabidopsis thaliana. *Plant Journal* **79**(3): 492-506.

Carpenter EJ, Matasci N, Ayyampalayam S, Wu S, Sun J, Yu J, Jimenez Vieira FR, Bowler C, Dorrell RG, Gitzendanner MA, et al. 2019. Access to RNA-sequencing data from 1,173 plant species: The 1000 Plant transcriptomes initiative (1KP). *Gigascience* **8**(10).

Chmelová D, Škulcová D, Ondrejovic M. 2019. Microbial xylanases and their inhibition by specific proteins in cereals. *Kvasny Prumysl* **65**(4): 127–133-127–133.

Chong SL, Koutaniemi S, Juvonen M, Derba-Maceluch M, Mellerowicz EJ, Tenkanen M. 2015. Glucuronic acid in Arabidopsis thaliana xylans carries a novel pentose substituent. *International Journal of Biological Macromolecules* **79**: 807-812.

Clough SJ, Bent AF. 1998. Floral dip: a simplified method for Agrobacterium-mediated transformation of Arabidopsis thaliana. *Plant Journal* **16**(6): 735-743.

Darriba D, Taboada GL, Doallo R, Posada D. 2011. ProtTest 3: fast selection of best-fit models of protein evolution. *Bioinformatics* **27**(8): 1164-1165.

Eddy SR. 2011. Accelerated Profile HMM Searches. *PLoS Comput Biol* **7**(10): e1002195.

Edgar RC. 2004a. MUSCLE: a multiple sequence alignment method with reduced time and space complexity. *BMC Bioinformatics* **5**: 113.

Edgar RC. 2004b. MUSCLE: multiple sequence alignment with high accuracy and high throughput. *Nucleic Acids Research* **32**(5): 1792-1797.

Evtuguin DV, Tomas JL, Silva AMS, Neto CP. 2003. Characterization of an acetylated heteroxylan from Eucalyptus globulus Labill. *Carbohydrate Research* **338**(7): 597-604.

Fu L, Niu B, Zhu Z, Wu S, Li W. 2012. CD-HIT: accelerated for clustering the next-generation sequencing data. *Bioinformatics* **28**(23): 3150-3152.

Giummarella N, Pu YQ, Ragauskas AJ, Lawoko M. 2019. A critical review on the analysis of lignin carbohydrate bonds. *Green Chemistry* **21**(7): 1573-1595.

Goubet F, Barton CJ, Mortimer JC, Yu XL, Zhang ZN, Miles GP, Richens J, Liepman AH, Seffen K, Dupree P. 2009. Cell wall glucomannan in Arabidopsis is synthesised by CSLA glycosyltransferases, and influences the progression of embryogenesis. *Plant Journal* **60**(3): 527-538.

Grantham NJ, Wurman-Rodrich J, Terrett OM, Lyczakowski JJ, Stott K, Iuga D, Simmons TJ, Durand-Tardif M, Brown SP, Dupree R, et al. 2017. An even pattern of xylan substitution is critical for interaction with cellulose in plant cell walls. *Nature Plants* **3**(11): 859-865.

Han MH, Liu YT, Zhang FL, Sun DF, Jiang JX. 2020. Effect of galactose side-chain on the self-assembly of xyloglucan macromolecule. *Carbohydrate Polymers* **246**.

Hefer C, Mizrachi E, Joubert F, Myburg A 2011. The Eucalyptus genome integrative explorer (EucGenIE): a resource for Eucalyptus genomics and transcriptomics. *BMC Proceedings*: Springer. 1-1.

Hurlbert JC, Preston JF, 3rd. 2001. Functional characterization of a novel xylanase from a corn strain of Erwinia chrysanthemi. *Journal of Bacteriology* **183**(6): 2093-2100.

Immelmann R, Gawenda N, Ramirez V, Pauly M. 2023. Identification of a xyloglucan beta-xylopyranosyltransferase from Vaccinium corymbosum. *Plant Direct* **7**(7): e514.

Izuno A, Hatakeyama M, Nishiyama T, Tamaki I, Shimizu-Inatsugi R, Sasaki R, Shimizu KK, Isagi Y. 2016. Genome sequencing of Metrosideros polymorpha (Myrtaceae), a dominant species in various habitats in the Hawaiian Islands with remarkable phenotypic variations. *Journal of Plant Research* **129**(4): 727-736.

Izuno A, Wicker T, Hatakeyama M, Copetti D, Shimizu KK. 2019. Updated Genome Assembly and Annotation for Metrosideros polymorpha, an Emerging Model Tree Species of Ecological Divergence. *G3 (Bethesda)* **9**(11): 3513-3520.

James CM, Barrett JA, Russell SJ, Gibby M. 2001. A rapid PCR based method to establish the potential for paternal inheritance of chloroplasts in Pelargonium. *Plant Molecular Biology Reporter* **19**: 163-167.

Katoh K, Standley DM. 2013. MAFFT multiple sequence alignment software version 7: improvements in performance and usability. *Molecular Biology and Evolution* **30**(4): 772-780.

Kim JY, Symeonidi E, Pang TY, Denyer T, Weidauer D, Bezrutczyk M, Miras M, Zollner N, Hartwig T, Wudick MM, et al. 2021. Distinct identities of leaf phloem cells revealed by single cell transcriptomics. *Plant Cell* **33**(3): 511-530.

Kong YZ, Pena MJ, Renna L, Avci U, Pattathil S, Tuomivaara ST, Li XM, Reiter WD, Brandizzi F, Hahn MG, et al. 2015. Galactose-depleted xyloglucan is dysfunctional and leads to dwarfism in Arabidopsis. *Plant Physiology* **167**(4): 1296-U1294.

Li W, Godzik A. 2006. Cd-hit: a fast program for clustering and comparing large sets of protein or nucleotide sequences. *Bioinformatics* **22**(13): 1658-1659.

Li XF, Jackson P, Rubtsov DV, Faria-Blanc N, Mortimer JC, Turner SR, Krogh KB, Johansen KS, Dupree P. 2013. Development and application of a high throughput carbohydrate profiling technique for analyzing plant cell wall polysaccharides and carbohydrate active enzymes. *Biotechnology for Biofuels* **6**:94.

Li XM, Cordero I, Caplan J, Molhoj M, Reiter WD. 2004. Molecular analysis of 10 coding regions from arabidopsis that are homologous to the MUR3 xyloglucan galactosyltransferase. *Plant Physiology* **134**(3): 940-950.

Lyczakowski JJ, Wicher KB, Terrett OM, Faria-Blanc N, Yu X, Brown D, Krogh K, Dupree P, Busse-Wicher M. 2017. Removal of glucuronic acid from xylan is a strategy to improve the conversion of plant biomass to sugars for bioenergy. *Biotechnology for Biofuels* **10**: 224.

Mizrachi E, Maloney VJ, Silberbauer J, Hefer CA, Berger DK, Mansfield SD, Myburg AA. 2015. Investigating the molecular underpinnings underlying morphology and changes in carbon partitioning during tension wood formation in Eucalyptus. *New Phytologist* **206**(4): 1351-1363.

Mortimer JC, Faria-Blanc N, Yu XL, Tryfona T, Sorieul M, Ng YZ, Zhang ZN, Stott K, Anders N, Dupree P. 2015. An unusual xylan in Arabidopsis primary cell walls is synthesised by GUX3, IRX9L, IRX10L and IRX14. *Plant Journal* **83**(3): 413-426.

One Thousand Plant Transcriptomes I. 2019. One thousand plant transcriptomes and the phylogenomics of green plants. *Nature* **574**(7780): 679-685.

Paes G, Berrin JG, Beaugrand J. 2012. GH11 xylanases: Structure/function/properties relationships and applications. *Biotechnology Advances* **30**(3): 564-592.

Paradis E, Schliep K. 2019. ape 5.0: an environment for modern phylogenetics and evolutionary analyses in R. *Bioinformatics* **35**(3): 526-528.

Patron NJ, Orzaez D, Marillonnet S, Warzecha H, Matthewman C, Youles M, Raitskin O, Leveau A, Farre G, Rogers C, et al. 2015. Standards for plant synthetic biology: a common syntax for exchange of DNA parts. *New Phytologist* **208**(1): 13-19.

Pena MJ, Kulkarni AR, Backe J, Boyd M, O'Neill MA, York WS. 2016. Structural diversity of xylans in the cell walls of monocots. *Planta* **244**(3): 589-606.

Pinto PC, Evtuguin DV, Neto CP. 2005. Structure of hardwood glucuronoxylans: modifications and impact on pulp retention during wood kraft pulping. *Carbohydrate Polymers* **60**(4): 489-497.

Rogowski A, Briggs JA, Mortimer JC, Tryfona T, Terrapon N, Lowe EC, Basle A, Morland C, Day AM, Zheng HJ, et al. 2015. Glycan complexity dictates microbial resource allocation in the large intestine. *Nature Communications* **6**: 7481.

Scheller HV, Ulvskov P. 2010. Hemicelluloses. *Annual Review of Plant Biol*ogy **61**: 263-289.

Schultink A, Cheng K, Park YB, Cosgrove DJ, Pauly M. 2013. The identification of two arabinosyltransferases from tomato reveals functional equivalency of xyloglucan side chain substituents. *Plant Physiology* **163**(1): 86-94.

Schultink A, Naylor D, Dama M, Pauly M. 2015. The Role of the Plant-Specific ALTERED XYLOGLUCAN9 Protein in Arabidopsis Cell Wall Polysaccharide O-Acetylation. *Plant Physiology* **167**(4): 1271-1283.

Shatalov AA, Evtuguin DV, Neto CP. 1999. (2-O-alpha-D-galactopyranosyl-4-O-methyl-alpha-D-glucurono)-D-xylan from Eucalyptus globulus Labill. *Carbohydrate Research* **320**(1-2): 93-99.

Shi D, Jouannet V, Agusti J, Kaul V, Levitsky V, Sanchez P, Mironova VV, Greb T. 2021. Tissue-specific transcriptome profiling of the Arabidopsis inflorescence stem reveals local cellular signatures. *Plant Cell* **33**(2): 200-223.

Simmons TJ, Mortimer JC, Bernardinelli OD, Pöppler AC, Brown SP, Deazevedo ER, Dupree R, Dupree P. 2016. Folding of xylan onto cellulose fibrils in plant cell walls revealed by solid-state NMR. *Nature Communications* **7**: 13902.

St John FJ, Hurlbert JC, Rice JD, Preston JF, Pozharski E. 2011. Ligand bound structures of a glycosyl hydrolase family 30 glucuronoxylan xylanohydrolase. *Journal of Molecular Biology* **407**(1): 92-109.

Stamatakis A. 2014. RAxML version 8: a tool for phylogenetic analysis and post-analysis of large phylogenies. *Bioinformatics* **30**(9): 1312-1313.

Tamura K, Shimada T, Kondo M, Nishimura M, Hara-Nishimura I. 2005. KATAMARI1/MURUS3 is a novel Golgi membrane protein that is required for endomembrane organization in Arabidopsis. *Plant Cell* **17**(6): 1764-1776.

Terrett OM, Dupree P. 2019. Covalent interactions between lignin and hemicelluloses in plant secondary cell walls. *Current Opinion in Biotechnology* **56**: 97-104.

Togashi H, Kato A, Shimizu K. 2009. Enzymatically derived aldouronic acids from Eucalyptus globulus glucuronoxylan. *Carbohydrate Polymers* **78**(2): 247-252.

Tryfona T, Bourdon M, Delgado Marques R, Busse-Wicher M, Vilaplana F, Stott K, Dupree P. 2023. Grass xylan structural variation suggests functional specialization and distinctive interaction with cellulose and lignin. *Plant Journal* **113**(5): 1004-1020.

Tryfona T, Liang HC, Kotake T, Kaneko S, Marsh J, Ichinose H, Lovegrove A, Tsumuraya Y, Shewry PR, Stephens E, et al. 2010. Carbohydrate structural analysis of wheat flour arabinogalactan protein. *Carbohydrate Research* **345**(18): 2648-2656.

Tryfona T, Stephens E. 2010. Analysis of carbohydrates on proteins by offline normal-phase liquid chromatography MALDI-TOF/TOF-MS/MS. *Plant Cell Wall: Methods and Protocols* **658**: 137-151.

Urbanikova L, Vrsanska M, Morkeberg Krogh KB, Hoff T, Biely P. 2011. Structural basis for substrate recognition by Erwinia chrysanthemi GH30 glucuronoxylanase. *FEBS Journal* **278**(12): 2105-2116.

Urbanowicz BR, Pena MJ, Ratnaparkhe S, Avci U, Backe J, Steet HF, Foston M, Li HJ, O'Neill MA, Ragauskas AJ, et al. 2012. 4-O-methylation of glucuronic acid in Arabidopsis glucuronoxylan is catalyzed by a domain of unknown function family 579 protein. *Proceedings of the National Academy of Sciences of the United States of America* **109**(35): 14253-14258.

Van Bel M, Diels T, Vancaester E, Kreft L, Botzki A, Van de Peer Y, Coppens F, Vandepoele K. 2018. PLAZA 4.0: an integrative resource for functional, evolutionary and comparative plant genomics. *Nucleic Acids Research* **46**(D1): D1190-D1196.

Vroemen S, Heldens J, Boyd C, Henrissat B, Keen NT. 1995. Cloning and characterization of the bgxA gene from Erwinia chrysanthemi D1 which encodes a beta-glucosidase/xylosidase enzyme. *Molecular Genetics and Genomics* **246**(4): 465-477.

Wei QQ, Yang Y, Li H, Liu ZW, Fu R, Feng HQ, Li C. 2021. The xyloglucan galactosylation modulates the cell wall stability of pollen tube. *Planta* **254**(6): 133-140.

Wilson LF, Neun S, Yu L, Tryfona T, Stott K, Hollfelder F, Dupree P. 2023. The biosynthesis, degradation, and function of cell wall β□xylosylated xyloglucan mirrors that of arabinoxyloglucan. *New Phytologist* **240** (6): 2353-2371.

Wu AM, Hornblad E, Voxeur A, Gerber L, Rihouey C, Lerouge P, Marchant A. 2010. Analysis of the Arabidopsis IRX9/IRX9-L and IRX14/IRX14-L pairs of glycosyltransferase genes reveals critical contributions to biosynthesis of the hemicellulose glucuronoxylan. *Plant Physiology* **153**(2): 542-554.

Yu L, Yoshimi Y, Cresswell R, Wightman R, Lyczakowski JJ, Wilson LFL, Ishida K, Stott K, Yu XL, Charalambous S, et al. 2022. Eudicot primary cell wall glucomannan is related in synthesis, structure, and function to xyloglucan. *Plant Cell* **34**(11): 4600-4622.

Zhang H, Yohe T, Huang L, Entwistle S, brown P, Yang Z, Busk PK, Xu Y, Yin Y. 2018. dbCAN2: a meta server for automated carbohydrate-active enzyme annotation. *Nucleic Acids Research* **46**(W1): W95-W101.

Zhao Z, Crespi VH, Kubicki JD, Cosgrove DJ, Zhong LH. 2014. Molecular dynamics simulation study of xyloglucan adsorption on cellulose surfaces: effects of surface hydrophobicity and side-chain variation. *Cellulose* **21**(2): 1025-1039.

Zhu L, Dama M, Pauly M. 2018. Identification of an arabinopyranosyltransferase from *Physcomitrella patens* involved in the synthesis of the hemicellulose xyloglucan. *Plant Direct* **2**(3): e00046.

Figure Legends

Figure 1. AT1G68470/XAPT1 from GT47 subclade A is a functional xylan arabinopyranosyltransferase. (a), PACE analysis of *Np*Xyn11A xylanase digests of alkali-extracted xylan from AIR of WT, the *xapt1* T-DNA insertion mutant, and three independent transgenic lines expressing *XAPT1* under the strong primary wall-specific promoter of *CESA3* in the *xapt1* background. (b), PACE analysis of *Bo*XynC xylanase digests of WT and *xapt1* mutant young stem. Xylo-oligosaccharide standard: X–X_6.

Figure 2. Trimmed phylogenetic tree of the XAPT subclade of GT47-A. Sequences grouped in the XAPT subclade of our previous GT47-A tree (Yu et al., 2022) were supplemented with HMMER and TBLASTN hits for XAPT-like sequences in Myrtales genomes. Following alignment, the phylogeny was inferred using RAxML. For rooting, *At*MUR3 was included as the outgroup. Due to the large number of sequences (106), we show only an abridged form of the tree here (displaying the more pertinent sequences), hence bootstrap values (from 100 pseudoreplicates) may underestimate the confidence of the splits shown. The full phylogeny can be viewed in Fig. S3.

Figure 3. Overexpression of *Eg*XLPT or *Eg*XAPT can decorate the glucuronoxylan with an additional sugar. (a), Expression of *Eg*XLPT and *Eg*XAPT under primary cell wall *CESA3* promoter can complement the *xapt1* xylan structure phenotype. Alkali-extracted xylan from 5-week-old young stem was digested with *Np*Xyn11A xylananase and analyzed by PACE. (b), Expression of *Eg*XLPT and *Eg*XAPT under secondary wall *IRX3* promoter in Arabidopsis WT can decorate most of the glucuronoxylan with an addition sugar. Alkali-extracted xylan from 8-week-old bottom stem was digested with *Bo*XynC xylanase and analysed by PACE. Xylo-oligosaccharide standard: X–X_6.

Figure 4. *Eg*XAPT and *Eg*XLPT exhibit different donor sugar specificities. AIR was extracted from 8-week-old bottom stems of either Arabidopsis WT plants or transgenic plants expressing *Eg*XAPT or *Eg*XLPT under the secondary cell wall-specific promoter of IRX3. Alkali-extracted xylan was then digested with *Bo*Xyn30C xylanase followed by GH115 glucuronidase. The products were labelled with 2-AA and analysed by MALDI-TOF MS.

Figure 5. Xylan structure in different *Eucalyptus dalrympleana* tissues. (a), Eucalyptus stems were sectioned into cortex, phloem, and xylem/sapwood. Major leaf vein tissue was not included for the leaf xylan analysis. Scale bar = 0.9 cm. (b), PACE analysis of *Bo*XynC

xylanase digests of AIR from different tissues. Xylo-oligosaccharide standard: $X–X_6$. $U^{Arap,Gal,[m]}X_n$ structures are labelled with arrows.

Figure 6. Distribution of xylan with decorated GlcA in different *Eucalyptus dalrympleana* tissues. AIR from different tissues was digested with *Bo*XynC xylanase followed by GH115 glucuronidase to remove the undecorated GlcA. The products were labelled with 2-AA and then analysed by MS.

Figure 7. Differences in GH30 xylanase active site residues may reflect differences in ability to accommodate substituted glucuronic acid sidechains. (a), Previously characterised active site of GH30 xylanase from plant pathogen *Dickeya chrysanthemi* (previously *Erwinia chrysanthemi*) strain D1 (Ec_DXyn30A; PDB: 2Y24). Bound aldotriuronic acid is shown in stick representation. The side chain of Tyr255, which forms a hydrogen bond with the GlcA C2 hydroxyl, is highlighted in orange. (b), Alignment segment of five GH30 xylanases, highlighting residues aligned to Tyr255 in Ec_DXyn30A. (c), Molecular phylogeny of GH30 subfamily 8 sequences downloaded from dbCAN2 (http://bcb.unl.edu/dbCAN2/). Sequences that display a tyrosine residue in the column aligned to Tyr255 are highlighted in orange; those that instead display leucine are highlighted in blue, while those with asparagine are highlighted in purple.

Figure 8. PACE gels to show the activities of different GH30 xylanases towards substituted glucuronoxylan. (a), PACE analysis of three GH30 xylanases-digests of xylan from *gux1 gux2* double mutant, which only contains primary cell wall glucuronoxylan. (b), AIR from the transgenic plants expressing *Eg*XAPT or *Eg*XLPT under the secondary cell wall-specific promoter of *IRX3* were used as the substrates. Alkali-extracted xylan was then digested with different GH30 and the corresponding modified GH30 enzymes. All the plant materials are 30-day-old young stem. Xylo-oligosaccharide standard: $X–X_6$.

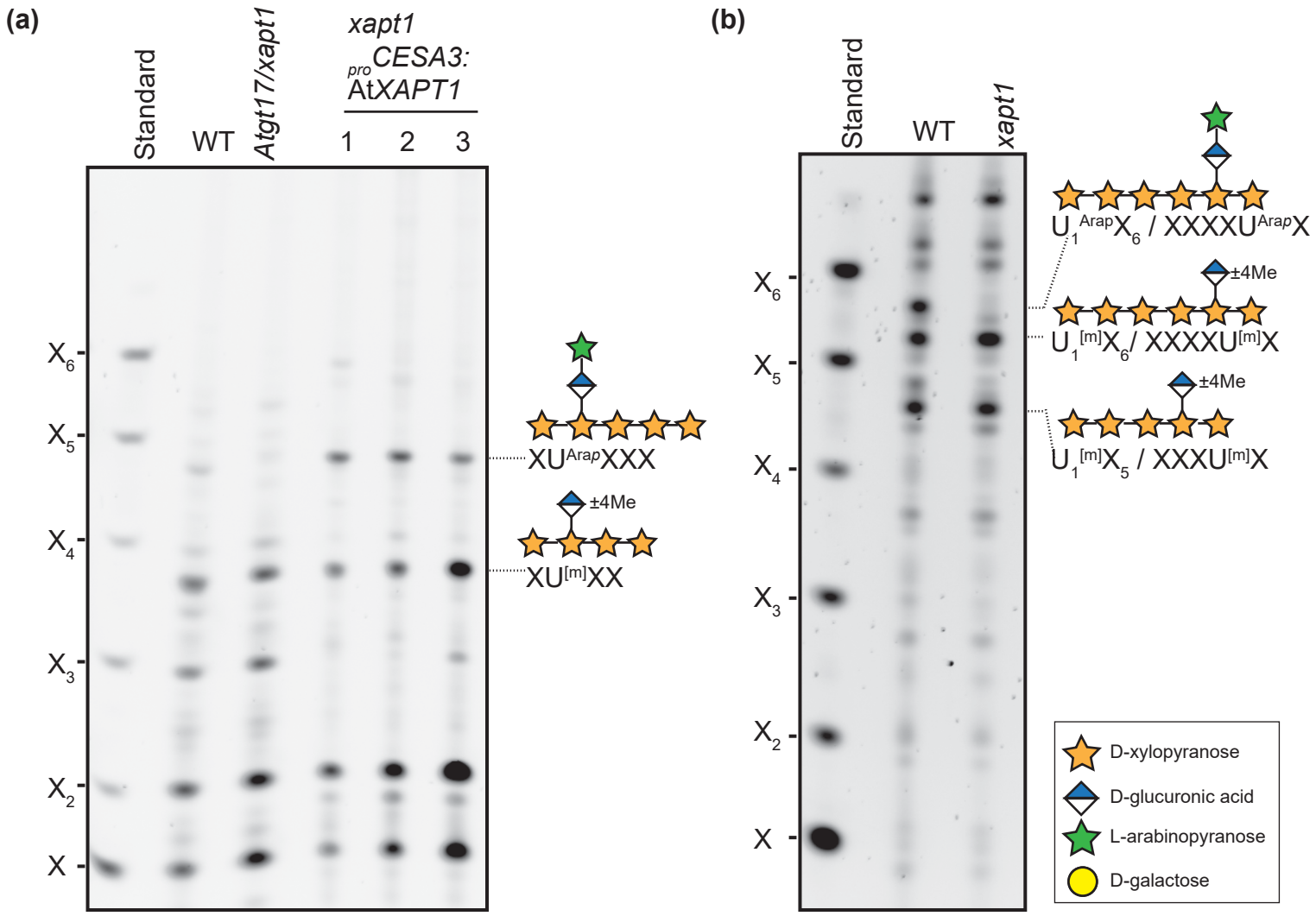
(a)
Standard
WT
Atgt17/xapt1
xapt1
proCESA3:
AtXAPT1
1
2
3
X6
X5
X4
X3
X2
X
XUArapXXX
±4Me
XU[m]XX
(b)
Standard
WT
xapt1
X6
X5
X4
X3
X2
X
U1ArapX6 / XXXXUArapX
±4Me
U1[m]X6/ XXXXU[m]X
±4Me
U1[m]X5 / XXXU[m]X
D-xylopyranose
D-glucuronic acid
L-arabinopyranose
D-galactose

Figure 1.

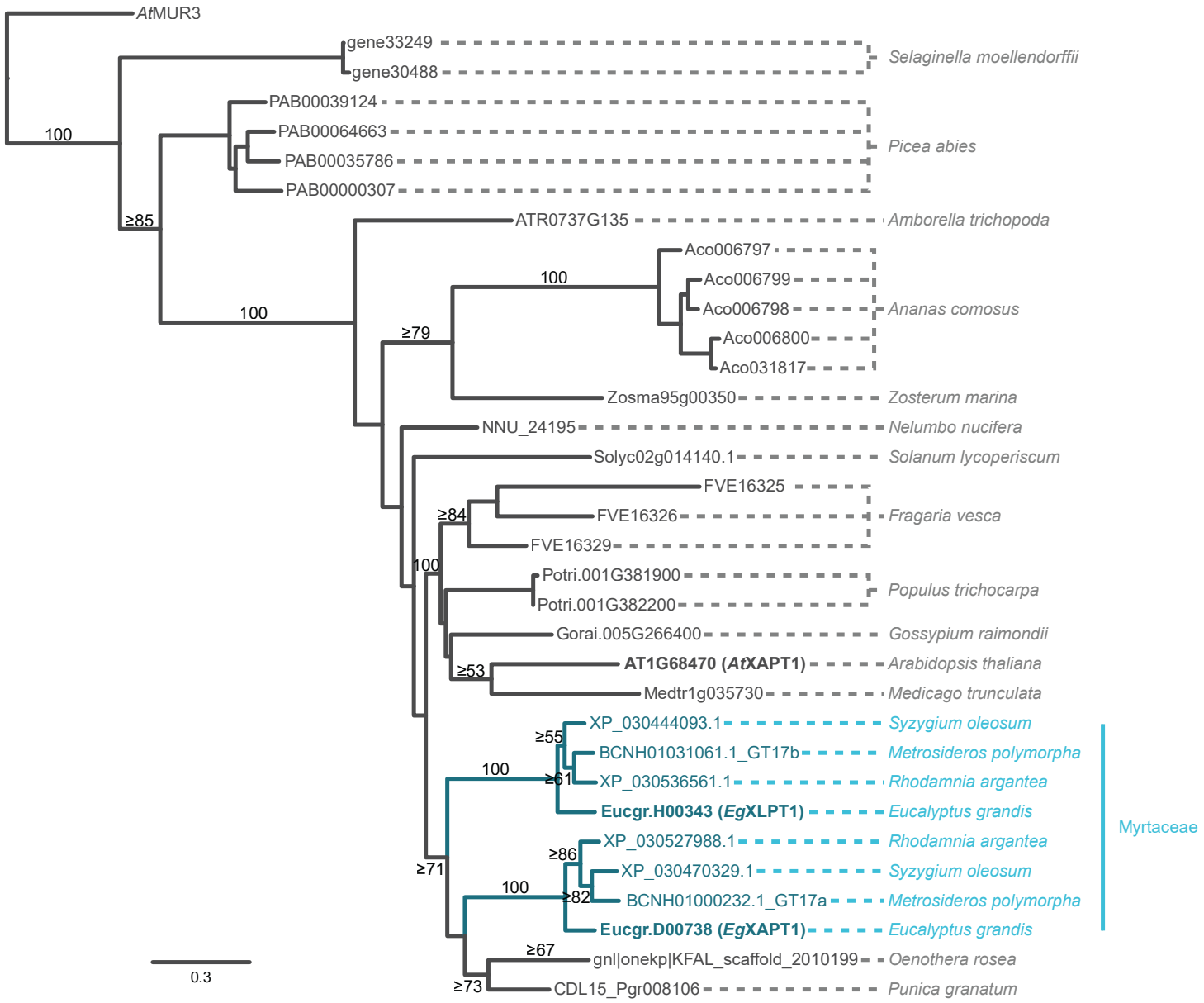
AtMUR3
gene33249
gene30488
Selaginella moellendorffii
PAB00039124
PAB00064663
PAB00035786
PAB00000307
Picea abies
100
≥85
ATR0737G135
Amborella trichopoda
Aco006797
Aco006799
Aco006798
Aco006800
Aco031817
Ananas comosus
100
100
≥79
Zosma95g00350
Zosterum marina
NNU_24195
Nelumbo nucifera
Solyc02g014140.1
Solanum lycoperiscum
FVE16325
FVE16326
FVE16329
Fragaria vesca
≥84
100
Potri.001G381900
Potri.001G382200
Populus trichocarpa
Gorai.005G266400
Gossypium raimondii
≥53
AT1G68470 (AtXAPT1)
Arabidopsis thaliana
Medtr1g035730
Medicago trunculata
XP_030444093.1
Syzygium oleosum
≥55
BCNH01031061.1_GT17b
Metrosideros polymorpha
100
≥61
XP_030536561.1
Rhodamnia argantea
Eucgr.H00343 (EgXLPT1)
Eucalyptus grandis
Myrtaceae
XP_030527988.1
Rhodamnia argantea
≥86
≥71
XP_030470329.1
Syzygium oleosum
100
≥82
BCNH01000232.1_GT17a
Metrosideros polymorpha
Eucgr.D00738 (EgXAPT1)
Eucalyptus grandis
≥67
gnl|onekp|KFAL_scaffold_2010199
Oenothera rosea
≥73
CDL15_Pgr008106
Punica granatum
0.3

Figure 2.

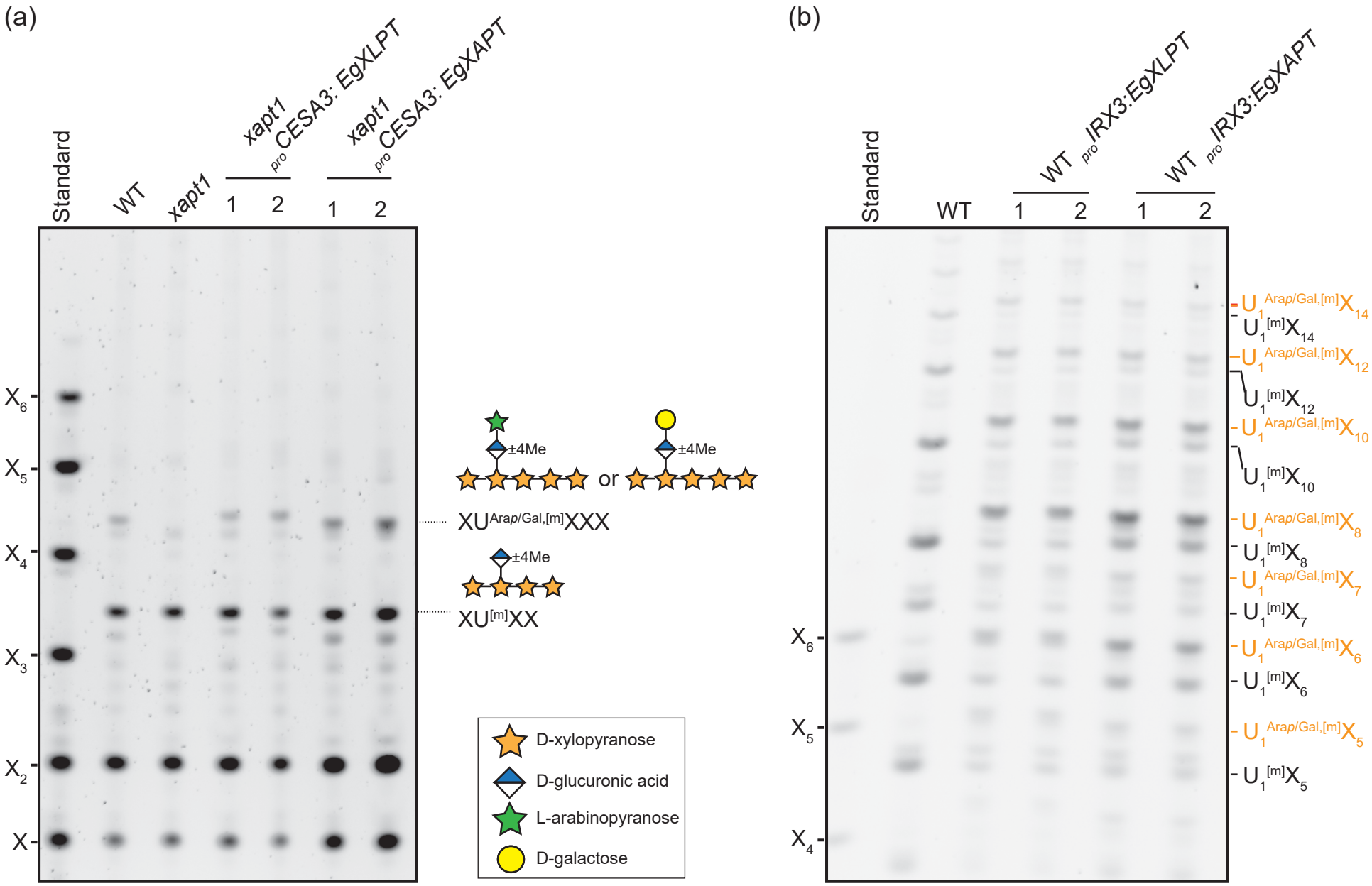
(a)
Standard
WT
xapt1
xapt1 pro CESA3: EgXLPT
1
2
xapt1 pro CESA3: EgXAPT
1
2
X6
X5
X4
X3
X2
X
±4Me
or
±4Me
XUArap/Gal,[m]XXX
±4Me
XU[m]XX
D-xylopyranose
D-glucuronic acid
L-arabinopyranose
D-galactose
(b)
Standard
WT
WT pro IRX3:EgXLPT
1
2
WT pro IRX3:EgXAPT
1
2
X6
X5
X4
U1Arap/Gal,[m]X14
U1[m]X14
U1Arap/Gal,[m]X12
U1[m]X12
U1Arap/Gal,[m]X10
U1[m]X10
U1Arap/Gal,[m]X8
U1[m]X8
U1Arap/Gal,[m]X7
U1[m]X7
U1Arap/Gal,[m]X6
U1[m]X6
U1Arap/Gal,[m]X5
U1[m]X5

Figure 3.

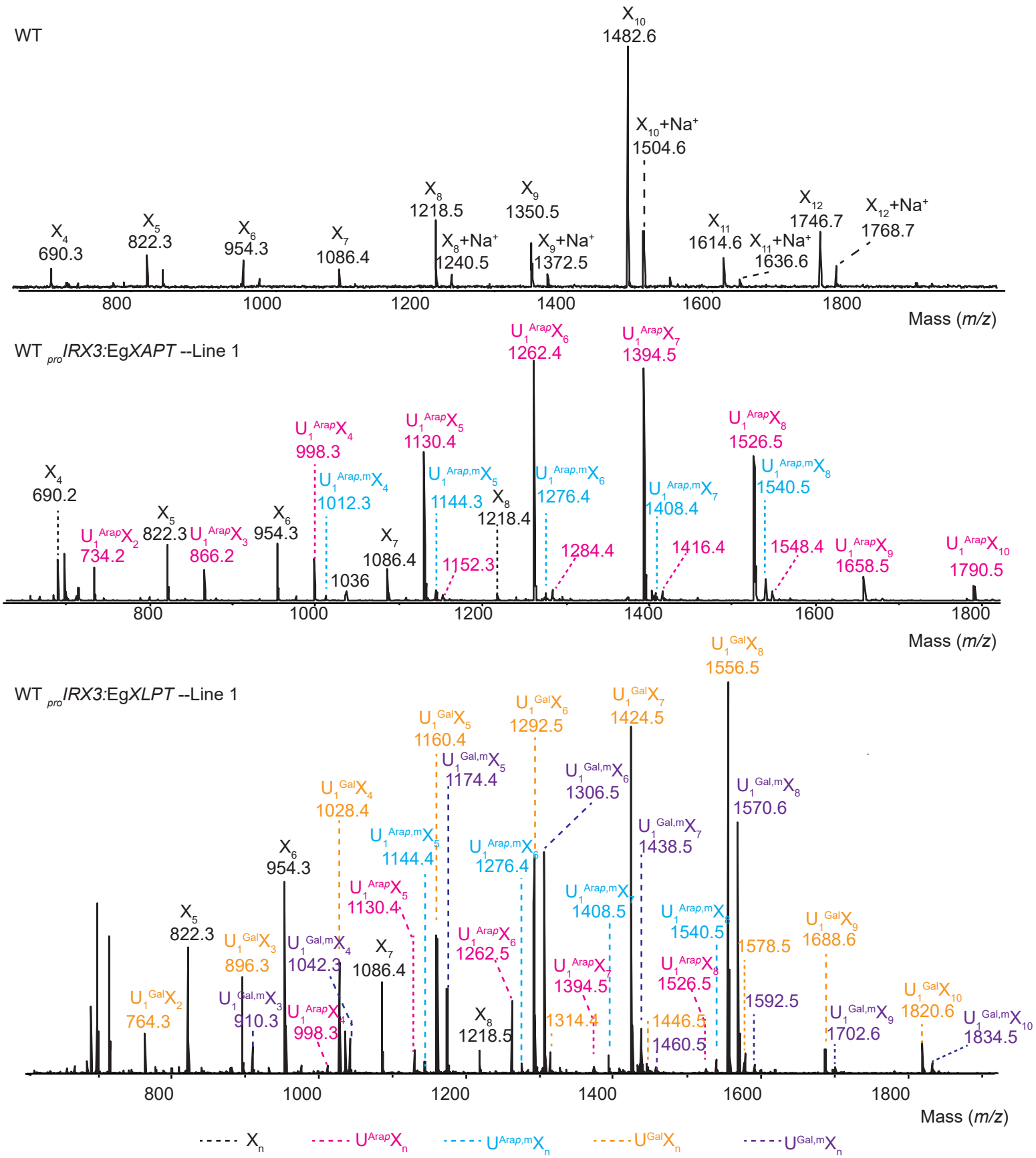
WT
X10 1482.6
X10+Na+ 1504.6
X4 690.3
X5 822.3
X6 954.3
X7 1086.4
X8 1218.5
X8+Na+ 1240.5
X9 1350.5
X9+Na+ 1372.5
X11 1614.6
X11+Na+ 1636.6
X12 1746.7
X12+Na+ 1768.7
800 1000 1200 1400 1600 1800
Mass (m/z)
WT proIRX3:EgXAPT --Line 1
X4 690.2
U1AraxX2 734.2
X5 822.3
U1AraxX3 866.2
X6 954.3
U1AraxX4 998.3
U1Arap,mX4 1012.3
1036
X7 1086.4
U1AraxX5 1130.4
U1Arap,mX5 1144.3
1152.3
X8 1218.4
U1AraxX6 1262.4
U1Arap,mX6 1276.4
1284.4
U1AraxX7 1394.5
U1Arap,mX7 1408.4
1416.4
U1AraxX8 1526.5
U1Arap,mX8 1540.5
1548.4
U1AraxX9 1658.5
U1AraxX10 1790.5
800 1000 1200 1400 1600 1800
Mass (m/z)
WT proIRX3:EgXLPT --Line 1
X5 822.3
U1GalX2 764.3
U1GalX3 896.3
U1Gal,mX3 910.3
X6 954.3
U1Gal,mX4 1042.3
U1AraxX4 998.3
U1GalX4 1028.4
X7 1086.4
U1AraxX5 1130.4
U1Arap,mX5 1144.4
U1Gal,mX5 1174.4
U1GalX5 1160.4
X8 1218.5
U1AraxX6 1262.5
U1Arap,mX6 1276.4
U1GalX6 1292.5
U1AraxX7 1394.5
1314.4
U1Arap,mX7 1408.5
U1Gal,mX6 1306.5
U1GalX7 1424.5
U1Gal,mX7 1438.5
U1AraxX8 1526.5
1446.5
1460.5
U1Arap,mX8 1540.5
U1GalX8 1556.5
U1Gal,mX8 1570.6
1578.5
1592.5
U1GalX9 1688.6
U1Gal,mX9 1702.6
U1GalX10 1820.6
U1Gal,mX10 1834.5
800 1000 1200 1400 1600 1800
Mass (m/z)
Xn
UAraxXn
UArap,mXn
UGalXn
UGal,mXn

Figure 4.

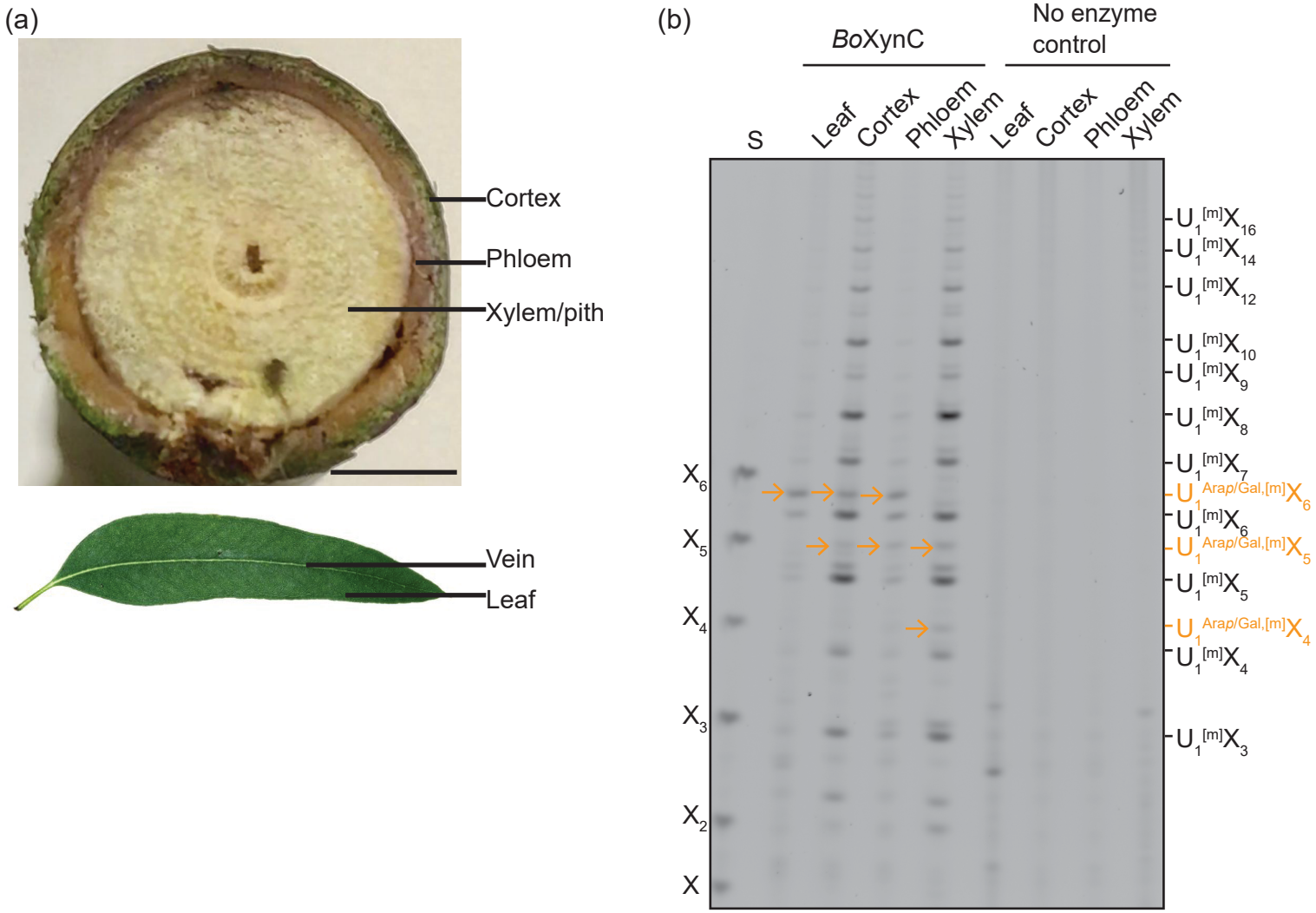
(a)
Cortex
Phloem
Xylem/pith
Vein
Leaf
(b)
BoXynC
No enzyme control
S
Leaf
Cortex
Phloem
Xylem
Leaf
Cortex
Phloem
Xylem
X6
X5
X4
X3
X2
X
U1[m]X16
U1[m]X14
U1[m]X12
U1[m]X10
U1[m]X9
U1[m]X8
U1[m]X7
U1Arap/Gal,[m]X6
U1[m]X6
U1Arap/Gal,[m]X5
U1[m]X5
U1Arap/Gal,[m]X4
U1[m]X4
U1[m]X3

Figure 5.

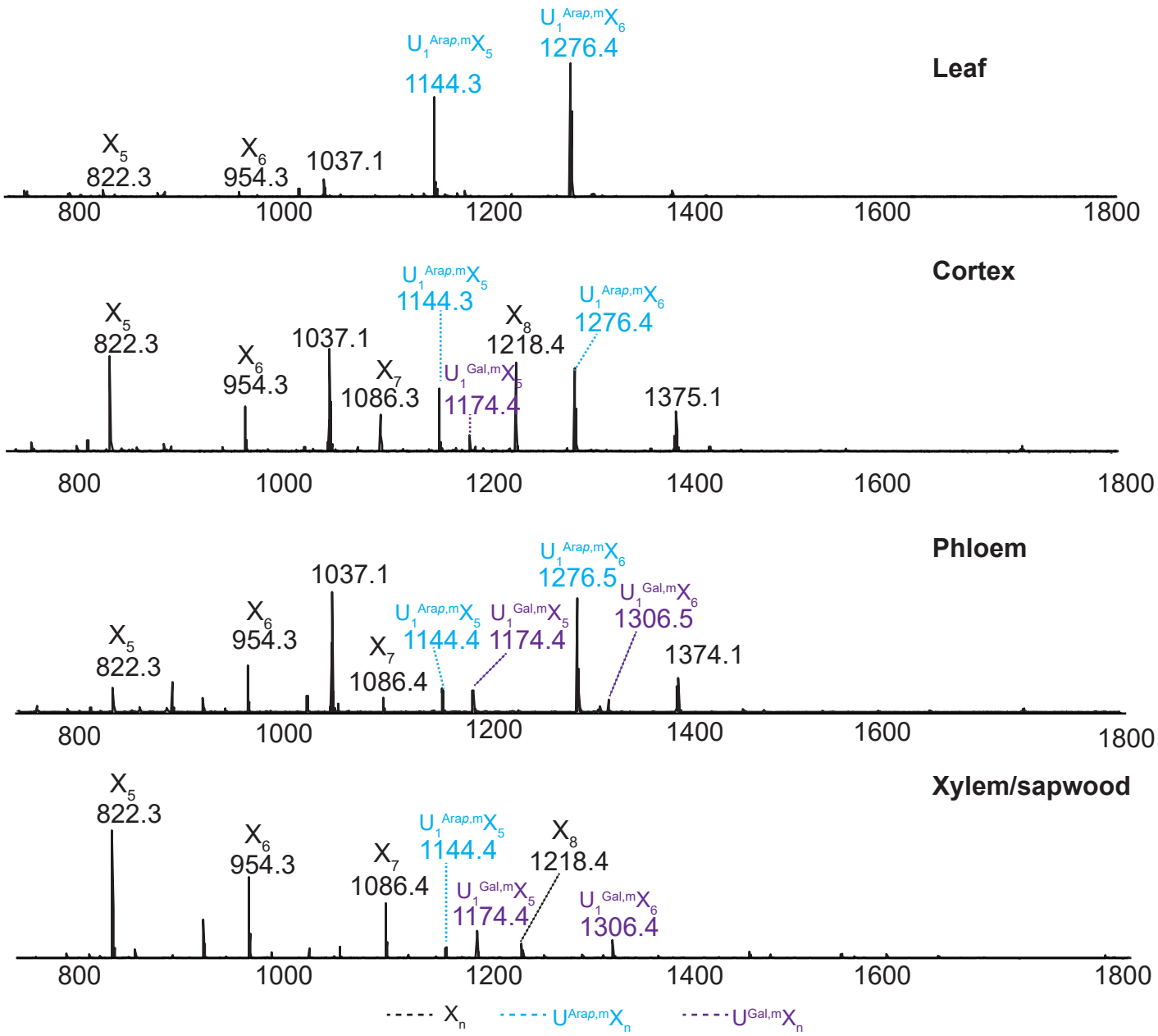
Leaf
X5 822.3
X6 954.3
1037.1
U1 Arap,m X5 1144.3
U1 Arap,m X6 1276.4
Cortex
X5 822.3
X6 954.3
1037.1
X7 1086.3
U1 Arap,m X5 1144.3
U1 Gal,m X5 1174.4
X8 1218.4
U1 Arap,m X6 1276.4
1375.1
Phloem
X5 822.3
X6 954.3
1037.1
X7 1086.4
U1 Arap,m X5 1144.4
U1 Gal,m X5 1174.4
U1 Arap,m X6 1276.5
U1 Gal,m X6 1306.5
1374.1
Xylem/sapwood
X5 822.3
X6 954.3
X7 1086.4
U1 Arap,m X5 1144.4
U1 Gal,m X5 1174.4
X8 1218.4
U1 Gal,m X6 1306.4
800
1000
1200
1400
1600
1800
Xn
UArap,m Xn
UGal,m Xn

Figure 6.

(a)

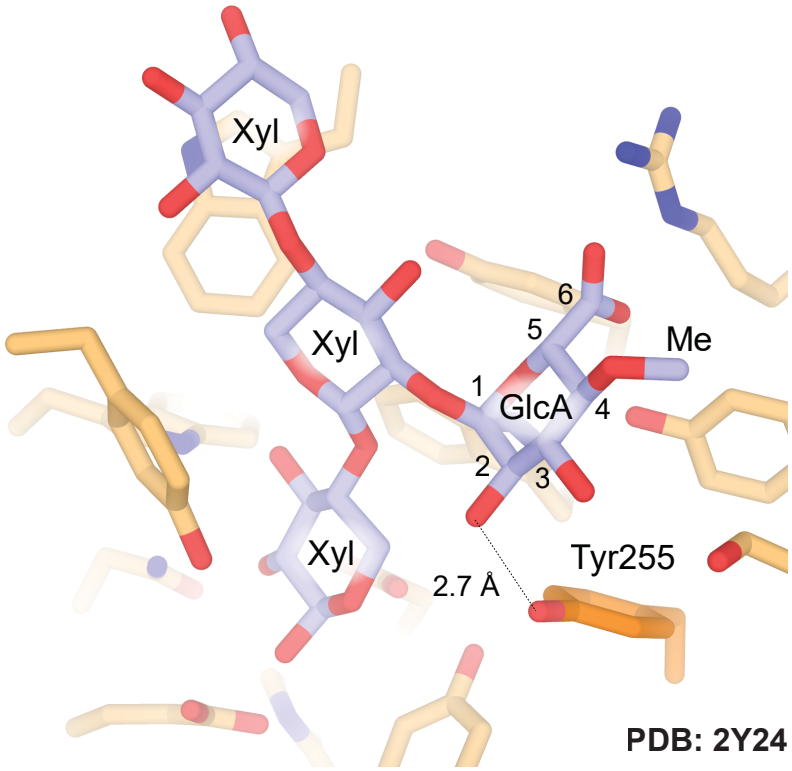

(b)

Ec$_D$ Xyn30A	QLWMTEH**Y**VDSKQSAN[263]
Ec$_P$ Xyn30A	QVWMTEH**L**VDSKQSAN[263]
*Bs*XynC	DLWMTEV**Y**YPNSDTNS[270]
*Ct*Xyn30A	ELWMTEV**Y**VPNSDSNS[268]
*Bo*XynC	TWWMTEH**L**FNDGENSD[382]
	**** . :. .

(c)

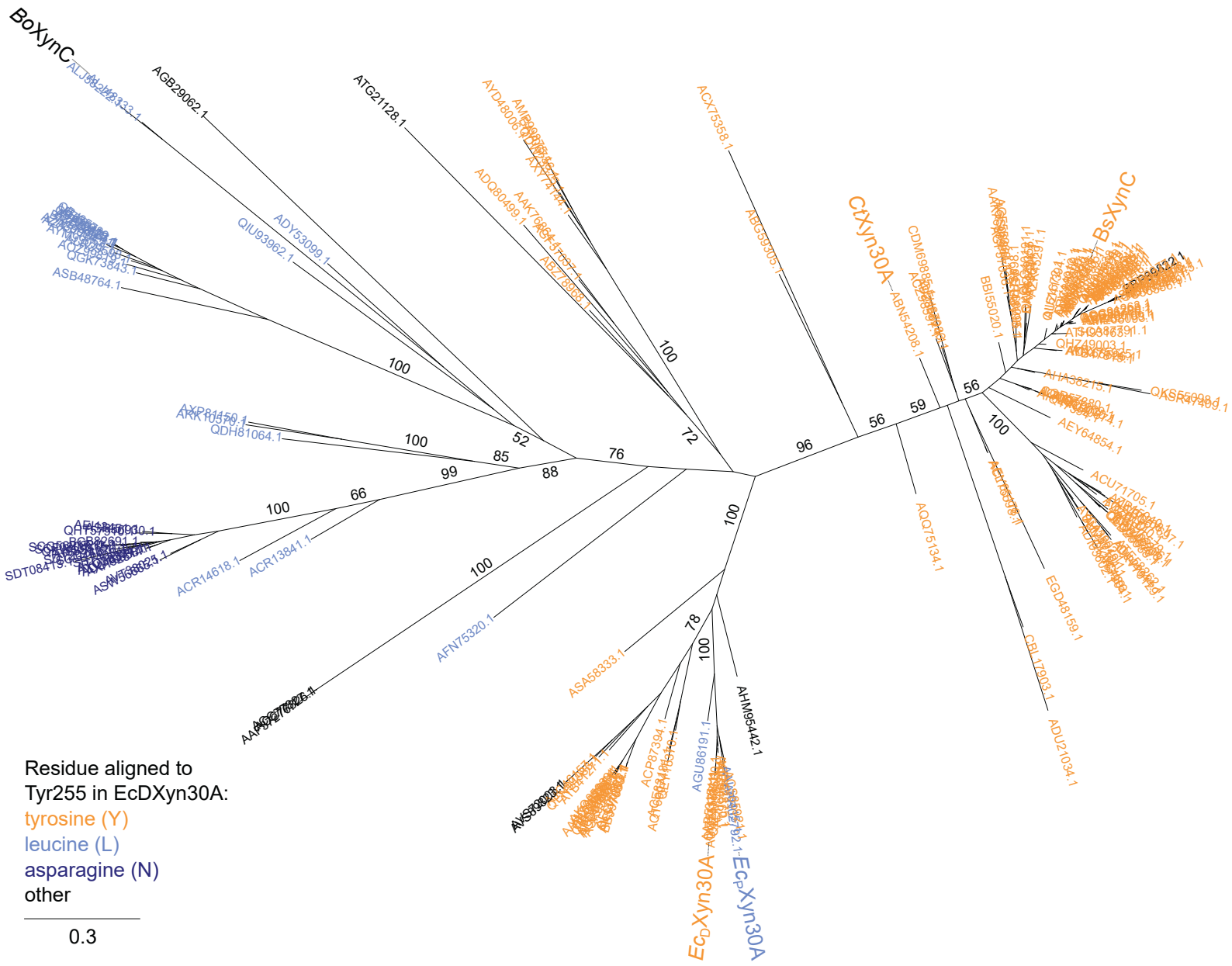

Figure 7.

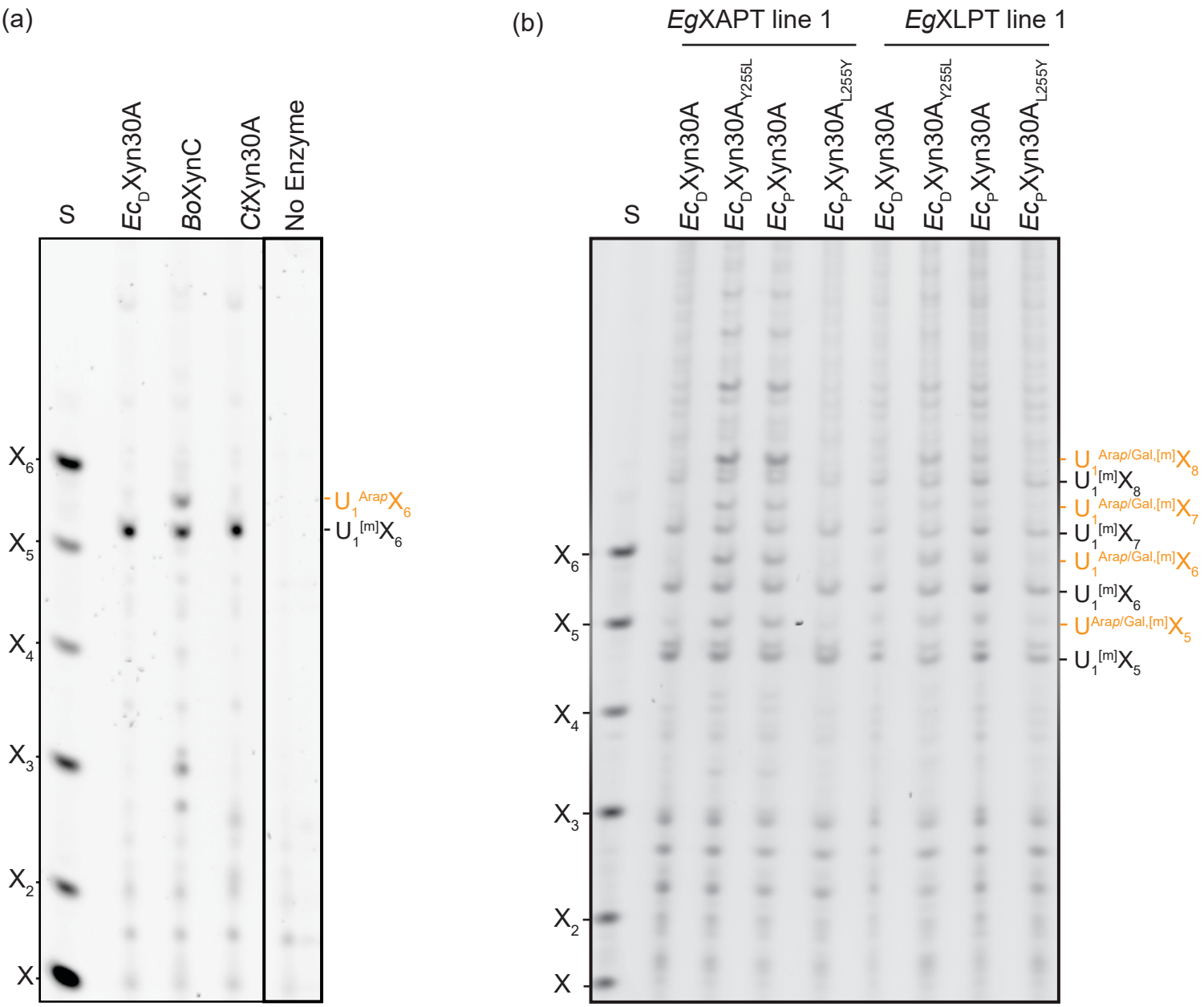
(a)
S
EcDXyn30A
BoXynC
CtXyn30A
No Enzyme
X6
X5
X4
X3
X2
X
U1 ArapX6
U1 [m]X6
(b)
EgXAPT line 1
EgXLPT line 1
S
EcDXyn30A
EcDXyn30AY255L
EcPXyn30A
EcPXyn30AL255Y
EcDXyn30A
EcDXyn30AY255L
EcPXyn30A
EcPXyn30AL255Y
X6
X5
X4
X3
X2
X
U1 Arap/Gal,[m]X8
U1 [m]X8
U1 Arap/Gal,[m]X7
U1 [m]X7
U1 Arap/Gal,[m]X6
U1 [m]X6
U Arap/Gal,[m]X5
U1 [m]X5

Figure 8